IJCESEN

ISSN : 2149-9144

International Journal of Computational and Experimental Science and ENgineering

Volume: 8 - Issue: 2 - 2022

ijcesen@gmail.com

Founder-Editor-in-Chief : Prof.Dr. İskender AKKURT

dergipark.org.tr/en/pub/ijcesen

Journal Info	
Web	dergipark.org.tr/en/pub/ijcesen
E-mail	ijcesen@gmail.com
ISSN	2149-9144
Frequency	March-July-November
Founded	2015
Journal Abbreviation	IJCESEN
Language	English-Turkish

Indexing/Abstracting Databases

ASOS indeks

INDEX COPERNICUS INTERNATIONAL

ISIFI – International Services for Impact Factor and Indexing

GENERAL IMPACT FACTOR
Universal Digital Object Information

Google Scholar

DRJI

ISI INTERNATIONAL Scientific Indexing

publons

Cosmos

SIA

J-Gate

WorldCat

ESJI Eurasian Scientific Journal Index
www.ESJIndex.org

JIF – Global Society for Scientific Research
JIFACTOR

CiteFactor
Academic Scientific Journals

Academic Resource Index
ResearchBib

Scientific Journal Impact Factor
TOGETHER WE REACH THE GOAL

Table of Contents

International Journal of Computational and Experimental Science and ENgineering (IJCESEN)
Vol. 8-No.2 (2022) pp. 25-31
http://dergipark.org.tr/en/pub/ijcesen

ISSN: 2149-9144

Research Article

Classification of Alzheimer Disease with Molecular Communication Systems using LSTM

Ibrahim ISIK[1]*

[1]Department of Electrical Electronics Engineering, Inonu University,44280, Malatya, Turkey
* **Corresponding Author** : ibrahim.isik@inonu.edu.tr **ORCID:** 0000-0003-1355-9420

Article Info:

DOI: 10.22399/ijcesen.1061006
Received : 21 January 2022
Accepted : 30 March 2022

Keywords

Nano communication
Number of received molecule
Deep learning
LSTM

Abstract:

Today, there are many diseases caused by cell or inter molecular communication. For example, a communication disorder in the nerve nano-network can cause very serious nervous system-related diseases such as Multiple Sclerosis (MS), Alzheimer's and Paralysis. Understanding these diseases caused by communication is very important in order to develop innovative treatment methods inspired by information technologies. In addition, many advanced environmental and industrial nano-sensor networks such as the development of biologically inspired Molecular Communication systems (MCs), cellular-accurate health monitoring systems, many medical applications such as the development of communication-capable nano-implants for nervous system diseases. Nano networks focused on communication between nano-sized devices (Nano Machines) is a new communication concept which is known as MCs in literature. In this study, on the contrary to the literature, a new Long Short-Term Memory (LSTM) based MC model has been used to analyse the proposed system. After obtained the number of received molecules for different number of Amyloid Beta (Aβ) which causes Alzheimer', a new method based on the LSTM model of deep learning is used for the classification of Aβ. Finally it is obtained that when the number of Aβ increases, the number of received molecules decrease. On a data set with five classes, experiments are conducted using LSTM. The proposed model's precision, accuracy and sensitivity values are determined as 97.05, 98.59 and 98.54 percent, respectively. The categorization procedure of the findings generated from the designed model appears to be performing well.

1. Introduction

In Molecular communication systems (MCs), chemical transceiver may be more favorable for implementation issues in transmitting information from transmitter to receiver or vice versa. In several fields, such as dentistry, bio-medical, environmental monitoring, industrial and defense purposes, these models can be used. Nearly all biological cells on their receiver surface use receptors to receive proteins, nutrients or other substances. A lot of studies have been carried out about the communication of nano-devices in recent years [1-6]. Generally, the transmitter (Tx) and receiver (Rx) parts are investigated to analyze transmitted and received molecules in a fluid media such as channel transfer function and the number of received molecules with a point transmitter and fully and half fully absorbing spherical receiver, pulse peak time and pulse amplitude concerning for the distance between transmitter and receiver, and attenuation, propagation delay, receptor models which are placed on the receiver randomly are considered as antenna using graphene and carbon nanotubes due to their prominent sensing capabilities for fixed Rx and Tx model of molecular communication via diffusion (MCvD) systems [7,8]. In [9], the proposed MCs model is analyzed for different distance values between Tx-Rx nanomachines and the diffusion constant of the environment. It is concluded from the study that, the number of received molecules increases with increasing diffusion constant and a decreasing distance between Tx and Rx. In [10], an adaptive

threshold mechanism, signal to interference, and bit alignment scheme are investigated for a simple and effective demodulation scheme for a mobile receiver with a speed of drift $V = 7.9 \times 10^{-4}$ *m/s* and diffusion coefficient of $D = 2.42 \times 10^{-10}$ m^2/s. The parameters such as the ratio of flow and receiver velocity and symbol interval are analyzed in terms of bit error rate (BER) using a fixed transmitter and mobile receiver. BER with or without ISI mitigation for different transmitting intervals is calculated and analyzed in this study [10]. The communication distance, which is described in MC systems as the distance between nanomachines, is one of the critical parameters that have a major impact on the quality of communication efficiency. In fixed MC, for instance, the CIR is defined as the expected number of molecules received, depending on the distance between nanomachines. The receiver can predict CIR and set an effective detection threshold in advance with knowledge of distance. The distance calculation and developing a mechanism between nanomachines should therefore be a primary justification for the design of MC systems using a neural networks or deep neural networks [11-14]. The hitting probability of transmitted molecules is generally analyzed at the receiver part in literature. The probability of a molecule being transmitted in a 1-D system is as follows:

$$f_{hit}^{1D}(t) = \frac{d}{\sqrt{4\pi D t^3}} e^{-\frac{d^2}{4Dt}}, \quad (1)$$

$$f_{hit}^{3D}(t) = \frac{r_r}{d+r_r} \frac{d}{\sqrt{4\pi D t^3}} e^{-\frac{d^2}{4Dt}} \ , \quad (2)$$

where r_r and d show the radius of the receiver, and distance from the transmitter to the surface of receiver, respectively.

In this study, firstly, the proposed MCs model is analyzed on the molecule reception rate of the model for different number of Aβ values separately. Secondly, after the number of received molecules is obtained for different number of Aβ, a new method based on the Long Short-Term Memory (LSTM) model of deep learning is used for the classification of number of Aβ.

2. Materials and Methods

Amyloid peptide is a protein produced by the cell itself in order to maintain its vital activities. However, with the breakdown of this protein by various enzymes, deterioration of the cell structure or overproduction, diseases for which no cure has yet been found arise. The most well-known of these is Alzheimer's disease, which causes forgetfulness in humans [14,15]. It is estimated that Alzheimer's disease is a disease caused by miscommunication or inability of cells to communicate. Amyloid beta (Aβ) peptides are formed by the degradation of amyloid precursor proteins (app), known as type 1 membrane protein, by β-secretase and γ-secretase enzymes [15], It is known that App is produced by many cells of living things, but precursor proteins produced by nerve cells in the brain cause Alzheimer's disease [14,15]. Molecular communication is being studied by many researchers within the scope of nano-bio systems in order to shed light on the treatment of diseases caused by the disruption of communication systems of these and similar cells [16]. Although it is not known exactly how the communication between cells is disrupted in the literature, as a result of some experimental studies on mice, it has been concluded that the Aβ 40-42 peptide accumulates between neurons more than normal and prevents the transfer of information from the donor to the receiver [17].

In this study, pure diffusive channel method is used for moving of NMs in the fluid media. [18-20]. A point transmitter, sphere receiver, transporting molecules, and receptors on the receiver make up the suggested MCs model. Between the transmitter and the receiver, MMs are used as information carriers as shown in Fig. 1. In a 3-D environment, the receiver is set at the origin (0, 0, 0) and the transmitter is randomly placed at a distance d from the receiver. Every time step, the position of the receiver is changed at random, while the position of the transmitter is changed after each bit duration. A fluid propagation medium surrounds both the transmitter and the receiver. The medium is thought to be unconstrained, allowing it to spread in all directions to infinity. After being discharged into the medium, where they propagate according to Brownian motion, the molecules may arrive at the receiver. The information molecules are absorbed by the spherical receiver's receptors with a radius of r s. The receiver absorbs a molecule that collides with one of the receptors on its surface. It bounces back if it collides with the receiver's surface without striking a receptor [21,22]. For the sake of simplicity, the suggested model ignores messenger molecule collisions, as stated in the literature. The cumulative number of received molecules for a spherical completely absorbing receiver is calculated analytically in Eq. 3. The absorption probability of a chemical in transition is presented in 3-D environment without taking into account the influence of receptors by the completely absorbing receiver until time t.

$$F_{hit}(t) = \frac{r_r}{r_0} erfc(\frac{d}{\sqrt{4Dt}}) , \quad (3)$$

where r_0 denotes the distance between the point transmitter and the receiver's center, t is the time after the molecule was released, and *erfc()* denotes the complementary error function [21].

Table 1. *System parameters.*

Radius of receiver, r_r	3.101 µm
Number of Aβ	5, 10, 15, 20 µm
Radius of receptor, r_s	0.01 µm
Number of receptor Number of transmitted molecules	7200 20000
Number of simulation	100
Diffusion constant of environment, D	79.4 μm^2/s

2.1 Long Short-Term Memory (LSTM)

Long Short-Term Memory (LSTM) networks are a form of Recurrent Neural Networks (RNN) [23]. The hidden layer of an LSTM neural network, also known as the LSTM cell, has a complex structure. As illustrated in Fig. 1, the LSTM cell is made up of three gates: the input gate, the forget gate, and the output gate [23,25], which control the flow of information through the cell and neural network. The LSTM model shown in figure 1, is a chain-like structure built of progressively constructed data [26,27].

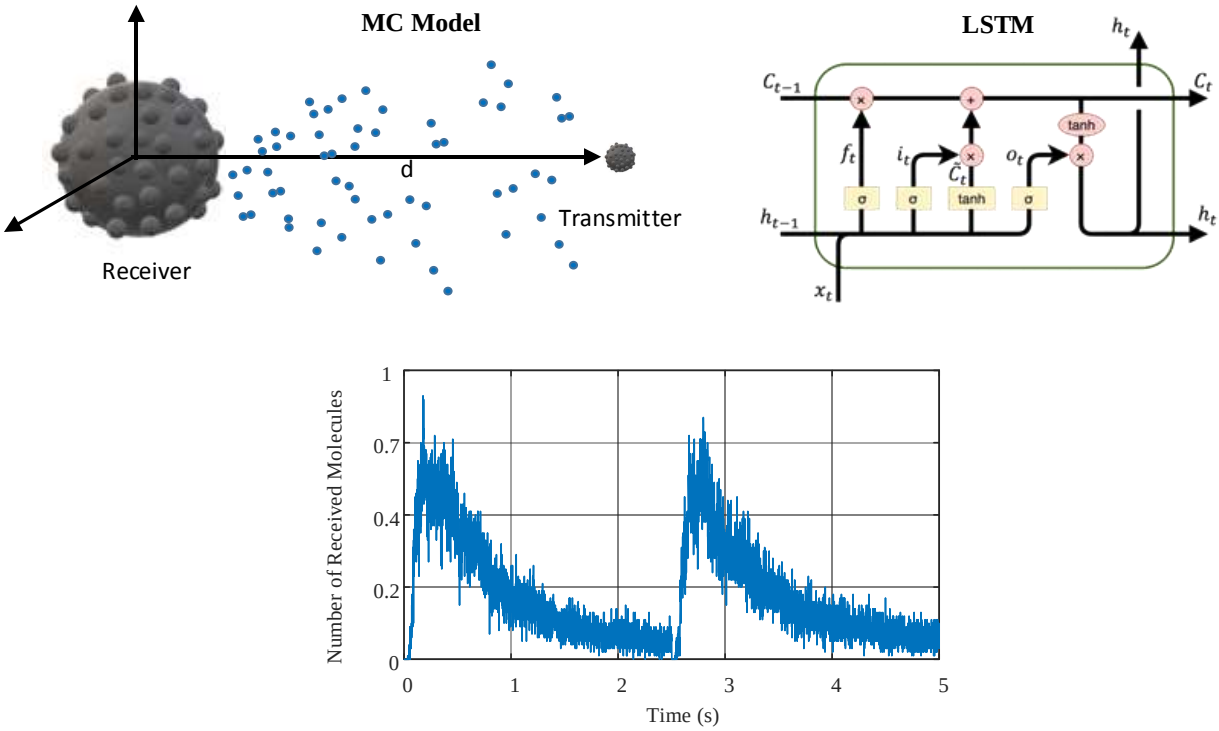

Figure 1. *The proposed MC model with LSTM.*

As shown in Eq. 4, the first step in processing an LSTM network is to determine the information to be taken from the cell (table 1). The sigmoid function awarded the data definition and exclusion process. The sigmoid function also determined which portion of the mine's output should be extracted. The forget gate layer, also known as ft, is a sigmoid layer that makes this decision: where h(t-1) is a vector that goes from 0 to 1 for each integer in the cell state $C_{(t-1)}$.

$$f_t = \sigma(W_F[h_{t-1}, X_t] + b_f) \quad (4)$$

where (W_F) and (b_f) are the weighting matrices of the forget gate and bias vector, respectively, and is the sigmoid function. The input gate of the LSTM is described in Eqs. 5-7. In Eq. 5, the new information (X_t) from the input gate layer is stored, and the cell state is also updated. There are two components to this. The "input gate layer," a sigmoid layer, chose which values would update or not (0 or 1), and the second layer is known as tanh. The tanh function in Eq. 6 produced a vector for the new candidate value (-1 to 1) and applied weight to the data provided (to push the values between 1 and 1). To update the new cell state, two values are multiplied. The following stages are to update the old memory state, C_{t-1}, into the new memory state, C_t, as shown in Eq. 7.

$$i_t = \sigma(W_i[h_{t-1}, X_t + b_i]), \quad (5)$$

$$N_t = tanh(W_n[h_{t-1}, X_t] + b_n), \quad (6)$$

$$C_t = C_{t-1} f_t + N_t i_t. \quad (7)$$

The cell states $C_{(t-1)}$ and C_t in the time interval between t-1 and t are $C_{(t-1)}$ and C_t, respectively. In Eq. 8, the sigmoid layer determined which parts of the current cell reach the output. The output of the sigmoid gate (O_t) is then multiplied by the new values (C_t) formed by the tanh layer, as shown in Eq. 9.

$$O_t = \sigma(W_0[h_{t-1}, X_t] + b_0) \quad (8)$$

$$h_t = O_t tanh(C_t) \quad (9)$$

W_0 and b_0 which are the weight matrix and bias vector of the output gate respectively.

The accuracy, precision, and sensitivity of the results obtained from the suggested method were assessed using assessment criteria. Eqs. 10-12 give the mathematical formulae for each of these evaluation criteria.

$$Accuracy = \frac{|TP|+|TN|}{|TP|+|FP|+|FN|+|TN|} \quad (10)$$

$$Precision = \frac{|TP|}{|TP|+|FP|} \quad (11)$$

$$Sensitivity = \frac{|TP|}{|TP|+|FN|} \quad (12)$$

In this study, the proposed methodology and main components for the classification of number of Aβ are analysed in detail. The number of Aβ, time and number of received molecule features are given as input to the LSTM model and then the specifications obtained from LSTM were classified by using Softmax.

3. Results

The recommended model is examined using MATLAB 2021. A PC with an Intel I95.1GHz processor, 64GB of memory, and an NVIDIA Quadro RTX 3000 GPU was also used to train and test the recommended model. The time, number of Aβ, and number of received molecules are given as inputs to the created two-layer LSTM model with 32 and 64 outputs. Figure 2 shows the fluctuation of LSTM features in two-dimensional coordinates (x and y), which represent two of the LSTM characteristics.

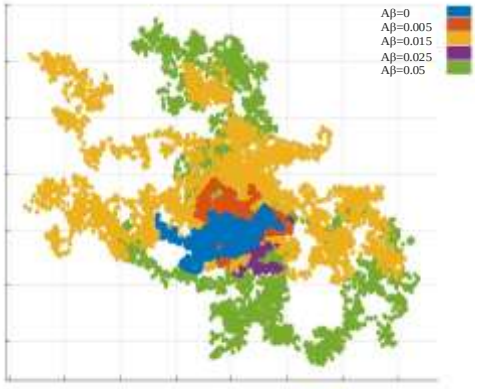

Figure 2. *2D Representation of LSTM Features.*

Half of the data is utilized for training and half is used for testing in the first trial. In the second trial, the data is separated for testing and training using the 10-fold cross validation process. Many parameters are used during the training phase to guarantee that the model is adequate and optimal. The measurements are carried out with varied batch sizes and learning rates for the optimum results. 32, 64, and 128 batch sizes have been chosen. The learning rates are also chosen as 0.1, 0.01, and 0.001 respectively. The epoch has been changed from 50 to 50. The accuracy and loss during training and testing are depicted in Figure 3.

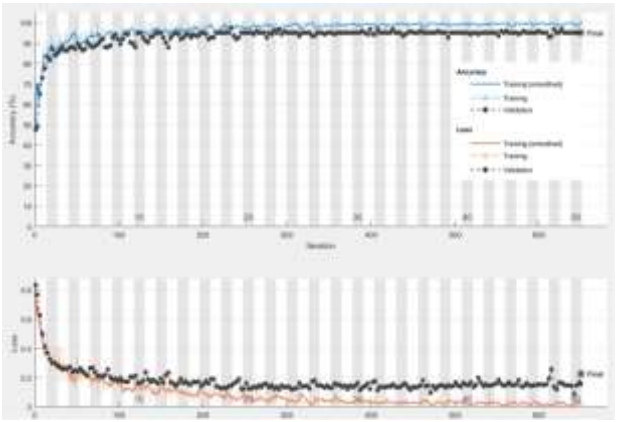

Figure 3. *Plots of accuracy and loss on training and validation sets.*

Table 2 shows the categorization results obtained by employing 50 percent for training and 50 percent for testing. The greatest accuracy of 97.05 percent is attained when the batch sizes are set to 128 and the learning rate is set to 0.001. The batch sizes were set to 64 and the learning rate was 0.1, yielding the maximum accuracy of 96.12 percent, and the batch sizes were set to 32 and the learning rate was 0.001, yielding the best accuracy of 96.14 percent.

Table 2. *Classification results obtained by splitting the data into 50% training and 50% test.*

	Batch -Size	Learn ing rate	Accuracy %	Precision %	Sensitivity %
LSTM		0.1	95.79	96.02	96.54
	32	0.01	95.59	96.02	95.82
		0.001	96.14	96.42	94.23
		0.1	96.12	96.68	96.52
	64	0.01	95.59	95.54	98.54
		0.001	95.41	96.92	97.50
		0.1	96.85	97.50	97.97
	128	0.01	95.92	97.90	96.98
		0.001	97.05	98.59	97.01

Table 3 displays the classification results obtained by utilizing the 10-k fold cross validation procedure to divide the data. When the batch sizes are set to 64 and the learning rate is set to 0.001, the maximum accuracy is achieved. The batch sizes were 32 and the learning rate was 0.001, resulting in a maximum accuracy of 97.99 percent, while the batch sizes were 128 and the learning rate was 0.01, resulting in the greatest accuracy of 97.75 percent. The confusion matrix and Receiver Operating Characteristic (ROC) curve for the best classification result are shown in Figures 4 and 5.

Table 3*. Classification results obtained by dividing the data with the 10-fold cross validation technique.*

	Batch-Size	Learning rate	Accuracy %	Precision %	Sensitivity %
LSTM		0.1	96.92	96.92	96.42
	32	0.01	96.88	97.79	95.29
		0.001	97.99	96.34	94.99
		0.1	96.66	97.39	99.09
	64	0.01	96.81	97.81	95.07
		0.001	98.57	96.54	96.90
		0.1	97.45	97.36	97.03
	128	0.01	97.75	97.53	96.14
		0.001	96.06	96.86	95.01

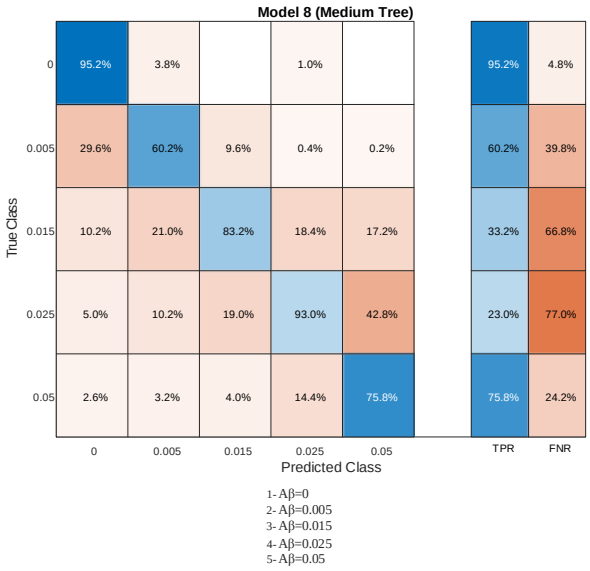

Figure 4. *Confusion Matrix.*

4. Conclusion and Future work

A new LSTM-based MC model is suggested in this paper to improve the hitting probability of MMs. For the lowest number of Aβ values, the number of received molecules is obtained higher. Although the proposed model has the lowest number of Aβ values, the number of received molecules is higher because certain molecules are absorbed by the number of Aβ

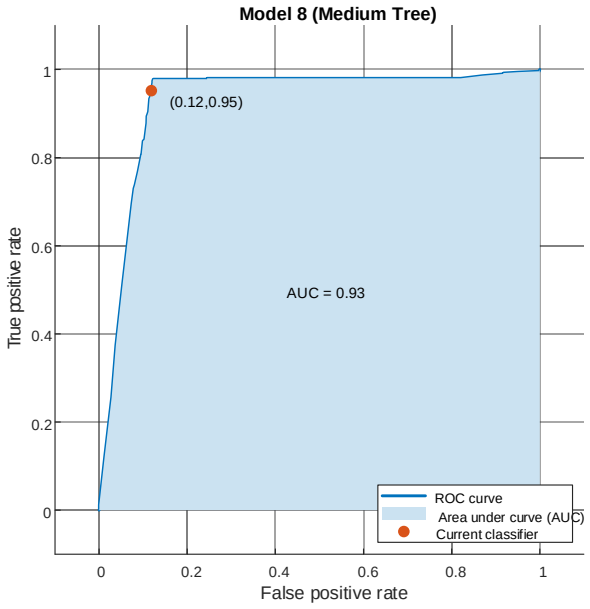

Figure 5. *ROC Curve.*

placed in the diffusion environment, which impacts communication quality. After obtaining the number of molecules received, the LSTM deep learning model was used to classify the number of Aβ values. More dynamic and biological systems can be constructed in the future by constructing a

proposed mobile MC model that takes into account more practical parameters such as precise drift velocity, vascular branching, and the influence of blood molecules. Also, using a deep neural network, estimate and optimization of the number of Aβ values in the environment can be considered to construct a more dynamic model with a lower signal to interference rate and a high receiver reception probability [28-30].

Author Statements:

- **Ethical approval:** The conducted research is not related to either human or animal use.
- **Conflict of interest:** The authors declare that they have no known competing financial interests or personal relationships that could have appeared to influence the work reported in this paper
- **Acknowledgement:** The authors declare that they have nobody or no-company to acknowledge.
- **Author contributions:** The authors declare that they have equal right on this paper.
- **Funding information:** The authors declare that there is no funding to be acknowledged.
- **Data availability statement:** The data that support the findings of this study are available on request from the corresponding author. The data are not publicly available due to privacy or ethical restrictions.

References

[1] T. H. Yutaka Okaie, Shouhei Kobayashi Tadashi Nakano, Yasushi Hiraoka, Tokuko Haraguchi, (2019). Methods and Applications of Mobile Molecular Communication. *Proc. IEEE*, 107(7) doi: 10.1109/JPROC.2019.2917625.

[2] Nariman Farsad, Weisi Guo†, Andrew Eckford (2014). Molecular Communication Link. Proceedings - IEEE INFOCOM DOI:10.1109/INFCOMW.2014.6849178
Conference: Computer Communications Workshops (INFOCOM WKSHPS), 2014 IEEE Conference on

[3] Benmansour, Djazia Leila et al. (2019). The nano scale bending and dynamic properties of isolated protein microtubules based on modified strain gradient theory," *Adv. Nano Res.*, 7(6):343-357 10.12989/anr.2019.7.6.443

[4] Ismail Bensaid, Ismail Bensaid, Ahmed Bekhadda and Bachir Kerboua (2018). Dynamic analysis of higher order shear-deformable nanobeams resting on elastic foundation based on nonlocal strain gradient theory," *Adv. Nano Res.*, 6(3):279-298 doi.org/10.12989/anr.2018.6.3.279

[5] Wael A. Altabey, Mohammad Noori, Ali Alarjani and Ying Zhao (2020). Nano-delamination monitoring of BFRP nano-pipes of electrical potential change with ANNs. *Adv. Nano Res.*, 9(1):1-13 doi.org/10.12989/anr.2020.9.1.001

[6] E. Isik and H. Toktamis, (2019). TLD characteristic of glass, feldspathic and lithium disilicate ceramics," *Luminescence*, 34(2):272–279 doi: 10.1002/bio.3605.

[7] H. B. Yilmaz, A. C. Heren, and T. Tugcu, (2014). 3-D Channel Characteristics for Molecular Communications with an Absorbing Receiver," *IEEE Commun. Lett.* https://arxiv.org/pdf/1404.4496.pdf

[8] Serena Lowa and Young-Seok Shon (2018). Molecular interactions between pre-formed metal nanoparticles and graphene families," *Adv. Nano Res.*, 6(4):357-375.

[9] E. Isik, (2020). Analyzing of the Viscosity by Using Artificial Neural Networks," *J. Phys. Chem. Funct. Mater.* 3(2):72–76.

[10] L. Lin, Q. Wu, M. Ma, and H. Yan, (2019). Concentration-based demodulation scheme for mobile receiver in molecular communication. *Nano Commun. Netw.*, 20:11–19 doi: 10.1016/j.nancom.2019.01.003.

[11] S. Huang, L. Lin, W. Guo, H. Yan, J. Xu, and F. Liu, (2020). Initial Distance Estimation and Signal Detection for Diffusive Mobile Molecular Communication. *IEEE Trans. Nanobioscience*, vol. 19(3):422–433 doi: 10.1109/TNB.2020.2986314.

[12] G. Wu and P. Tseng, (2021). A Deep Neural Network-Based Indoor Positioning Method using Channel State Information. pp. 290–294.

[13] C. M. A. Niitsoo, T. Edelhäußer, E. Eberlein, N. Hadaschik. (2018). A Deep Learning Approach to Position Estimation from Channel Impulse Responses," *Sensors*, 19(5):1064 doi: 10.3390/s19051064.

[14] N. Farsad and A. Goldsmith, (2018). Neural Network Detectors for Sequence Detection in Communication Systems. https://doi.org/10.1109/TSP.2018.2868322

[15] D. J. Selkoe *et al.* (1996). The role of APP processing and trafficking pathways in the formation of amyloid β-protein. *Ann. N. Y. Acad. Sci.*, 777(617):57–64. doi: 10.1111/j.1749-6632.1996.tb34401.x.

[16] Y. Zhou *et al.*, (2017). Amyloid beta: structure, biology and structure-based therapeutic development," *Acta Pharmacol. Sin.*, 38(9):1205–1235. doi: 10.1038/aps.2017.28.

[17] M. T. Barros, W. Silva, and C. D. M. Regis, (2018). The Multi-Scale Impact of the Alzheimer's Disease in the Topology Diversity of Astrocytes Molecular Communications Nanonetworks. Available: http://arxiv.org/abs/1810.09294.

[18] H. A. Pearson and C. Peers, (2006). Physiological roles for amyloid β peptides. *The journal of Physiology.* 1:5-10. doi: 10.1113/jphysiol.2006.111203.

[19] Q. Wu, L. Lin, Z. Luo, and H. Yan, (2017). Bit alignment scheme for mobile receiver in molecular communication," *Int. Conf. Ubiquitous Futur.*

Networks, ICUFN, pp. 750–752, doi: 10.1109/ICUFN.2017.7993892.

[20] Walsh, Frank (2013) *Protocols for Molecular Communication Nanonetworks.* PhD thesis, Waterford Institute of Technology.

[21] E. Isik, (2021). Analyzing of the diffusion constant on the nano-scale systems by using artificial neural networks," *AIP Adv.*, 11(10) doi: 10.1063/5.0067795.

[22] I. Isik, (2022). How Mobility of Transmitter and Receiver Effect the Communication Quality. *AIP Advances* 12(2):025205 DOI:10.1063/5.0082856

[23] A. Tomar and N. Gupta (2020). Prediction for the spread of COVID-19 in India and effectiveness of preventive measures. *Sci. Total Environ.*, 728:138762doi:10.1016/J.SCITOTENV.2020.138762.

[24] S. Hochreiter and J. Schmidhuber. (1997). Long Short-Term Memory. *Neural Comput.*, 9(8):1735–1780 doi: 10.1162/neco.1997.9.8.1735.

[25] A. A. Chowdhury, K. T. Hasan, and K. K. S. Hoque. (2021). Analysis and Prediction of COVID-19 Pandemic in Bangladesh by Using ANFIS and LSTM Network. *Cognit. Comput.*, 13(3):761–770 doi: 10.1007/s12559-021-09859-0.

[26] K.Vijayaprabakaran and K.Sathiyamurthy (2020). Towards activation function search for long short-term model network: A differential evolution based approach," *J. King Saud Univ. - Comput. Inf. Sci.*, (in press) doi: https://doi.org/10.1016/j.jksuci.2020.04.015.

[27] X. Glorot and Y. Bengio, (2010). *Understanding the difficulty of training deep feedforward neural networks.* Tirteenth international conference on artificial intelligence and statistics. 249–256.

[28] M. B. Er, E. Isik, and I. Isik (2021). Parkinson's detection based on combined CNN and LSTM using enhanced speech signals with Variational mode decomposition. *Biomed. Signal Process. Control* 70:103006 doi: 10.1016/J.BSPC.2021.103006

[29] I. Isik, H. B. Yilmaz, and M. E. Tagluk, (2017 September 16-17). *A Preliminary Investigation of Receiver Models in Molecular Communication via Diffusion* [Conference presentation abstract]. 2nd International Conference on Artificial Intelligence and Data Processing (IDAP17), Malatya, Türkiye

[30] E. Isik, I. Isik, and H. Toktamis, (2021). Analysis and estimation of fading time from thermoluminescence glow curve by using artificial neural network. *Radiat. Eff. Defects Solids* 176(9-10):765-776 doi: 10.1080/10420150.2021.1954000.

International Journal of Computational and Experimental Science and ENgineering (IJCESEN)

Vol. 8-No.2 (2022) pp. 32-39
http://dergipark.org.tr/en/pub/ijcesen

ISSN: 2149-9144

Research Article

Determination of Theoretical Fracture Criteria of Layered Elastic Composite Material by ANFIS Method from Artificial Intelligence

Arzu ÇİLLİ[1*], Murat BEKEN[2], Nursaç KURT[3]

[1]Yıldız Technical University, Science and Arts Faculty, Department of Physics, 34220, Istanbul-Turkey
***Corresponding Author** : **Email:** acilli@yildiz.edu.tr - **ORCID**: 0000-0002-0596-3637

[2]Bolu Abant İzzet Baysal University, Faculty of Engineering, Department of Computer Engineering, 14030, Bolu-Turkey
Email: murat.beken@ibu.edu.tr - **ORCID**: 0000-0001-9995-1321

[3]Istinye University, Faculty of Engineering, Department of Software Engineering, Istanbul-Turkey
Email: nursac.kurt@istinye.edu.tr - **ORCID**: 0000-0002-9338-0174

Article Info:

DOI: 10.22399/ijcesen.1077328
Received : 22 February 2022
Accepted : 30 March 2022

Keywords

Elastic Composite Material
Theoretical Fracture Criteria
Anfis
Sugeno

Abstract:

The theoretical breaking boundary of the composite elastic composite material consisting of two is otropichomogeneous layers was investigated. Three-dimensional theory of elasticity and a fragment edhomogeneous body model were used to find the theoretical breaking limit. The defects of this material, which has local defects, are of the same length hand is changing with the angle β. The purpose of the articles was to examine the effect of theoretical refraction criterion limit values on the change of the angle β. It has been observed that the theoretical refraction limit values obtained for four different composite materials increase as the angle art increases. In this study, the change values with the β angle of the theoretical refraction limit obtained in other our article were recovered from the artificial intelligence of the MATLAB platform by ANFIS (Sugeno) method. It was seen that the values obtained with the Anfis method are the same with the theoretical results.

1. Introduction

Determination of the theoretical fracture limit as a result of compressing composite materials under pressure is of great importance in theoretical and practical terms [1-3]. In this study, researchers were conducted for the layered composite consisting of two materials with local folds in its structure [4,5]. The limit of the theoretical fracture limit is standard within the scope of various material properties of elastic layer composites in one-way compression [6,7]. It should be noted that one of the main reasons for the breakage of one-way composites under single-axis compression along the matrix elements of the composite material is the stabilization loss in the material structure [6-9]. It is assumed that the local imperfection region of each reinforcing layer of this material is sin-phase and covers the same range along the layers. However, it shows that the initial defect regions in its structure have a certain movement of all layers of the material according to each other. Therefore, in the article [10,11], research was developed for cases where the elastic layers that are supplements act according to each other in local initial defect regions. As a result of these procedures, the changes in the angle of the fracture criteria of different elastic materials obtained were created by artificial intelligence ANFIS method. As a result of this method, the accuracy and learning of the system has been tested.

2. Theoretical Method of The Problem

The structural form of the material, which has local curvature in its structure and is in the form of a sin-phase of the curved cellules between the layers, is given in Fig.1. It is seen in Fig.1 that composite material consisting of alternate layers of two materials is under pressure along equally dispersed infinity reinforcement layers [10]. It will be assumed that the reinforcing (matrix) layers are placed on the planes parallel to the Ox_1x_3 plane and the thickness of each filling layer is constant. Moreover, it is assumed that the local imperfection regions of the

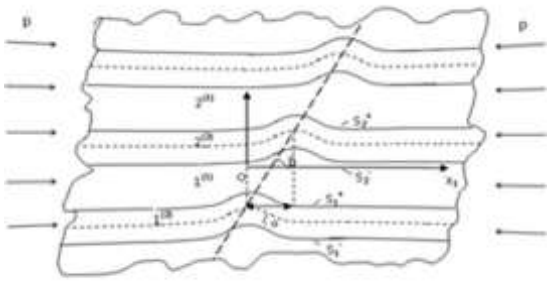

Figure.1 *A structure of the considered composite material with inclined local insignificant imperfection*

reinforcing layers move according to each other in the direction of the Ox_1 axis.
The moving length is

$$l_0 = 2H^{(1)} + H^{(2)} tg\beta \qquad (1)$$

selected as. Where $2H^{(1)}$, $H^{(2)}$ is the thickness of the reinforcing (matrix) layer and the angle β is shown in Fig.1. β=0 is considered as in the articles [10,11]. The values related to the matrix layer are shown with the upper indices (1) and those related to the filler are shown with the upper indices (2). It is assumed that the material of the layers of filler layers is only elastic composites (1).
In the Solution Method and the finding of the Theoretical Fracture Criteria, nonlinear exact balance equations of elasticities theory were used, and a fragmented homogeneous body model was applied.
Thus, for each selected layer, we write the equilibrium equations, mechanical and geometrical relations as follows [7-9].

$$\frac{\partial}{\partial x_{jm}^{(k)}}\left[\sigma_{jn}^{m(k)}\left(\delta_i^n + \frac{\partial u_{im}^{(k)}}{\partial x_{nm}^{(k)}}\right)\right] = 0 \quad ; \text{i, j, n =1,2; k=1,2} \qquad (2)$$

$$\sigma_{ij}^{m(k)} = \lambda^{(k)}\theta^{m(k)}\delta_i^j + 2\mu^{(k)}\varepsilon_{ij}^{m(k)}, \theta^{m(k)} = \varepsilon_{11}^{m(k)} + \varepsilon_{22}^{m(k)} \qquad (2.a)$$

$$2\varepsilon_{ij}^{m(k)} = \frac{\partial u_j^{m(k)}}{\partial x_{jm}} + \frac{\partial u_j^{m(k)}}{\partial x_{im}} + \frac{\partial u_n^{m(k)}}{\partial x_{im}^{(k)}}\frac{\partial u_n^{m(k)}}{\partial x_{jm}^{(k)}} \qquad (2.b)$$

Between each layer of the fill and matrix layers, the values for the zero and first approaches obtained before by using these equations and determining the contact conditions [6,7] are written [6,7] the values for the zero-approach given in [6.7] are shown to be determined from the non-linear equation. The linear equations obtained from the equation (2, 2a, 2b) are by determining the approach from the first order. Determining the values from the first approximation is reduced to solving the problem. For solution of this problem, we use the exponential Fourier transform,

$$f_F\ (s, x_2) = \int_{-\infty}^{+\infty} f(x_1, x_2) e^{-isx_1} dx_1 \qquad (3)$$

After the expression of the Fourier transformation of the sought-after values is determined, the relationship between the problem parameters is given as follows.

$$det\|\alpha_{nm}\| = 0 \qquad (4)$$

It is explained by determining the inverse Fourier transform.

$$f(x_1\ , x_2) = \frac{1}{2\pi}\int_{-\infty}^{+\infty} f_F\,(s\,, x_2)\, e^{isx_1}\, ds \qquad (5)$$

The roots of the equation coincide with the individual points of the appropriate function (3). As a result, the equation (4) is considered the order of the singuness of the function in (5). The integral defined here by (5) can be calculated using a well-known algorithm. Because the calculation of integral is done within the scope of Cauchy basic theory. In this case, (5) integral has no meaning and the corresponding force.

$$\frac{dp}{d(sH^2)} = 0 \qquad (6)$$

The definition that is also satisfactory for the corral determined from the equation can be called "critical force" (4). According to equation (6), the critical force equation corresponds to the local minimum (or maximum) value of the function that provides it. The resulting critical force values are taken as "Theoretical Fracture Criteria" since these values are not linked to the initial local defect mode and wave generation shape parameter. Numerical results showing the fracture criteria using the equation (6) and the effect on the values of the angle and fracture criterion for various parameters of the problem were solved numerically using PC and by bisection method [11]. These results are given in Table-1. Table-1 shows the fracture criteria obtained according to the changing angle values when using different elastic layer materials. As a result, the aim of the study was to examine the effect of angle and varying length on the values of the theoretical fracture limit. According to these results, theoretical fracture limit values were found to increase with the length of movement. This length is expressed by the angle shown in Fig.1.

Table.1 *Fracture limit values according to β angle change of different materials*

β	β(rad)	$\eta^{(2)}$ =0.5	$\eta^{(2)}$ =0.3	$\eta^{(2)}$ =0.2	$\eta^{(2)}$ =0.05
0	0	0,3302	0,2368	0,2079	0,1458
5	0,0872	0,3451	0,248	0,2172	0,1462
10	0,1744	0,3909	0,2802	0,2457	0,147
15	0,2616	0,4705	0,3371	0,2954	0,148
20	0,3488	0,5898	0,4224	0,3699	0,149
25	0,4361	0,7577	0,5427	0,4707	0,149
30	0,5233	0,9885	0,7082	0,5774	0,149
35	0,6105	1,304	0,9354	0,681	0,148
40	0,6977	1,7415	1,2025	0,771	0,146
45	0,785	2,3591	1,4424	0,8329	0,146

3. Method

3.1 Fuzzy Logic

Fuzzy logic is to process the values obtained by using the data with certain algorithms and to remove the result values by using certain mathematical functions depending on each rule it will create as a result. It was developed because of very valuable logic studies against Aristotle's two valuable logic proposals. Fuzzy logic derives results by considering the values between these two valuable logics and expresses the sizes with variables that are less, very, slightly, medium, long, normal, as appropriate for the verbal language. Allows trading with intermediate values (such as 0.3, 0.92) instead of 0-1 values [12].

A blurry process (fuzzy process) consists of three separate units.

1. Fuzzification unit
2. Rule processing unit
3. Clarification unit

In the flowchart shown in Fig. 2, the data from the stream is changed by taking it into a scale here, and this scaling event can also be called blur. This process can also be explained as follows, each of the incoming information is assigned a membership value and converted into a linguistic structure and bound by the rules [13]. Thus, numerical values are obtained according to the structure of incoming data

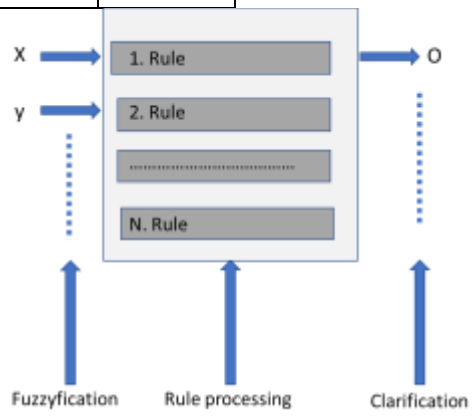

Figure.2 *General Representation of fuzzy system structure*

logical propositions and the results are sent to the rinser unit. In the rinser process, another scale change is performed in the fuzzy set, and the blurry information becomes real numbers [14,15].

3.2 Artificial Neural Network

Artificial neural networks are tools used in machine learning and are systems inspired by the learning of the human brain. It can obtain new data using the characteristics of the brain such as learning, remembering. The simulation between the biological nerve cell and the artificial neural network is given in Fig.3. According to this analogy, artificial neural networks can also be expressed as simulations of the biological nervous system. In the artificial neural networks cell seen in Fig.4, the input data and weights are multiplied in the artificial neural networks network, which has n inputs, creating bias

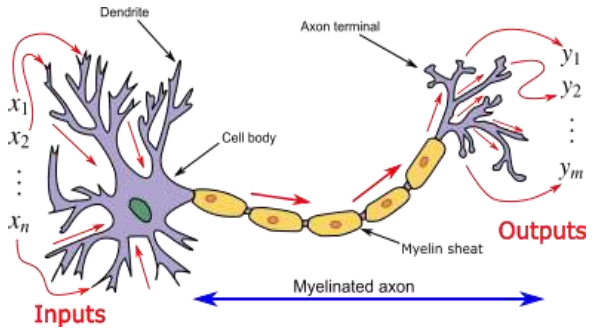

Figure.3 *Biological nerve cell and artificial neural network*

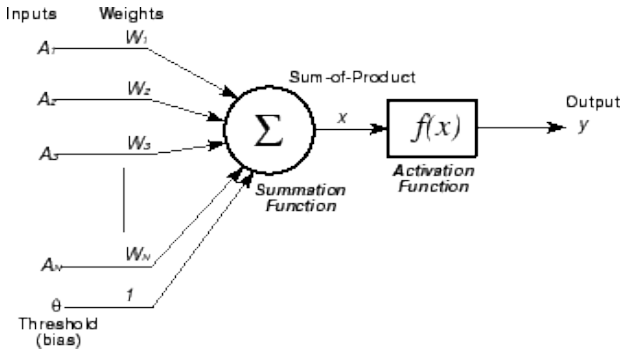

Figure.4 *Artificial neural network cell*

in its total function. The resulting net data is processed in the activation function. As a result of corrections in the Resulting Threshold value, activation is obtained.

3.3 Adaptive Neuro-Fuzzy Inference System – Anfis

Adaptive fuzzy neural networks system - Anfis (Adaptive Network Based Fuzzy Inference System) structure is a structure based on nerve layers formed because of its adaptation from the human brain, and they perform their duties with a certain function in the network on the given neurons. The structure of the ANFIS is fuzzy logic and artificial neural networks work as a hybrid [16]. Intuitive inferences of fuzzy logic and learning models of artificial neural networks work as a whole [17]. An ANFIS structure with two inputs in the first degree is shown in Fig.5. ANFIS has a five-layer structure, and these layers and their functions are as follows [18].

Layer 1: Node numbers are synchronized depending on the number of entries. In these nodes, the inputs are expressed as precursor parameters with a membership function.

Layer 2: The number of rules is created as much as the number of nodes in the structure. The rules of the outputs on the node show the degree of weight. The values entered the node express the values of the membership functions.

Layer 3: In this layer, the data coming to the nodes shows the degrees of weight, while the outputs express normalized weight grades. The main purpose of this layer is to normalize the rule weights.

Layer 4: All nodes are known to be adaptive, and the function of these nodes is a function in the Sugeno System. The functions functioning in this layer are of the first degree and perform the rinsing of the data.

Layer 5: In this layer, which is the last layer in our system, the values of non-blurred outputs are expressed.

Input and output parameters are the basic parameters of this five-tier system. First, the designated training data set is introduced to the designed artificial neural network. The system establishes a functional relationship between inputs and outputs with the best-tested training algorithm used and learning takes place. This process is done, optimization process. The sum of error squares is obtained by looking at the difference between the output of the system model and the output of the training data set. It is aimed to determine the optimum values of the parameters used by finding the cases where this total value, which is accepted as the error function, is minimum [16,19].

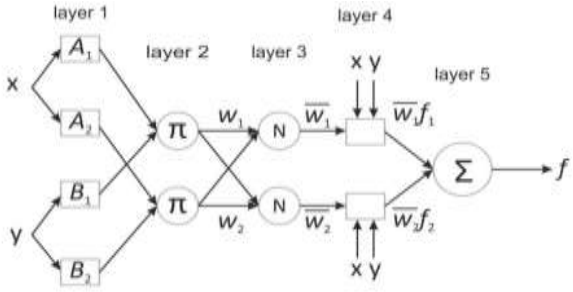

Figure.5 *An Anfis structure with two first-degree inputs and two rules*

3.4 Sugeno

Takagi – Sugeno fuzzy logic or Sugeno fuzzy logic was first used in 1985. The blurring of input variables and fuzzy logic operations are the same as Mamdani fuzzy modelling. The difference between the two methods is in the output membership functions. Output membership functions are linear or constant in Sugeno type fuzzy modelling as shown in Fig.6. When output membership functions are fixed, they are called zero degrees and when the first degree is in the form of the correct equation, they are called the first degree Sugeno fuzzy model.

Thus, the Sugeno-type fuzzy model is more complex and more impression-like than the Mamdani-type fuzzy model [20]. The advantages of the Sugeno-type blurred model are listed below; It is very suitable for calculation. Linear techniques can be used to control non-linear systems. It works well with optimization and adaptive techniques and improves results by optimizing output parameters. It has guaranteed continuity of the output surface. It is well suitable for mathematical analysis. Disadvantages of sugeno-type fuzzy model; When high sugeno fuzzy modelling is used, it has a very complex structure. Increasing the number of inputs and subsets make it difficult to train data, and the number of soncul parameters that must be determined to achieve the results increases. It's not very in accordance with human intuition [21].

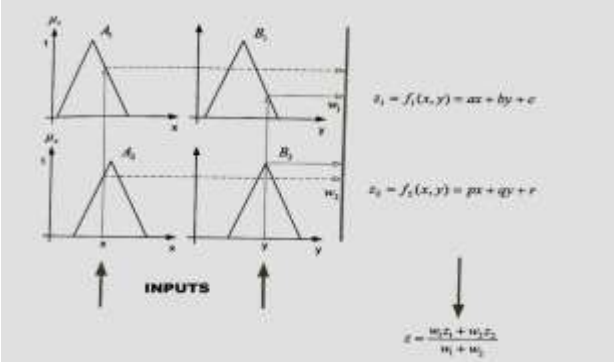

Figure.6 *Takagi-Sugeno Inference*

4. Results and Discussions

4.1 Applied of Anfis

A dataset based on input and output is generally needed to implement the ANFIS method. Depending on the number and type of membership function selected, the established model is created using a learning algorithm. The number of iterations during ANFIS applications is an important parameter. A value is determined that allows adequate and necessary improvements to be made. The error graph that occurs because of training the system with ANFIS is given in Fig.7. It is seen that the error value of the system during the training phase is 4.0119e-05. The resulting values resulting from the testing of the data with the control set were obtained as shown in Fig.8. The average error value of RMSE obtained by testing the network was determined as 4.0119e-05. Through the Fuzzy Logic Designer application, we can see how many inputs, outputs, and variables the system has and their names. There are 5 inputs in our system in Fig.9. These are β, β(radian), $\eta^{(2)}$ =0.5, $\eta^{(2)}$ =0.3, $\eta^{(2)}$ =0.2

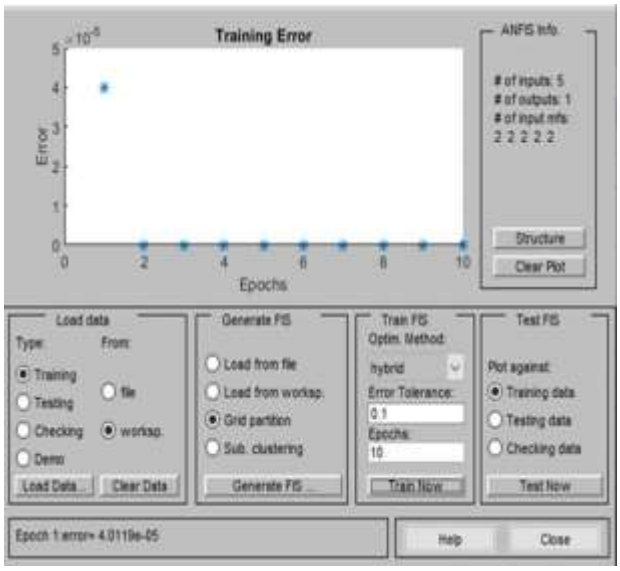

Figure.7 *Error chart caused by the training a network*

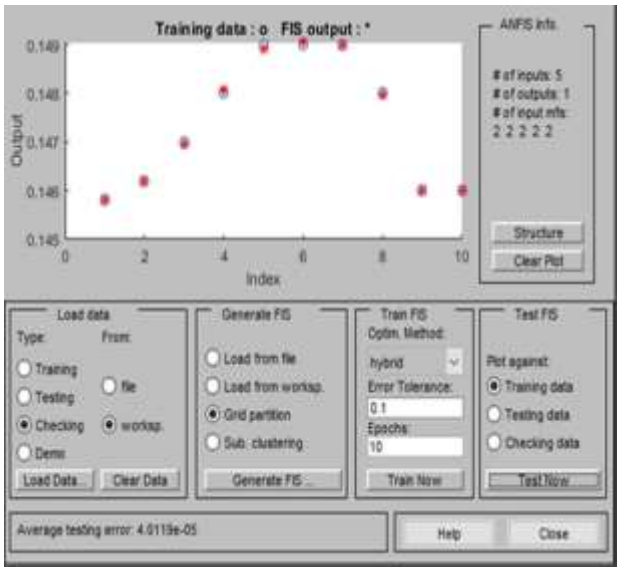

Figure.8 *Comparison of actual values and system-estimated values*

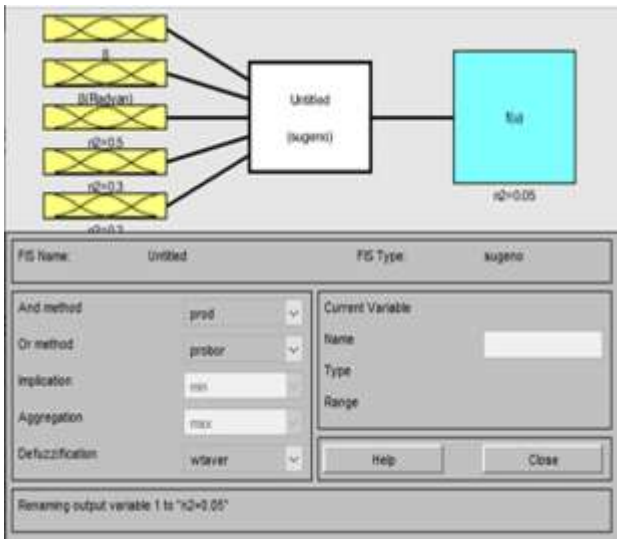

Figure.9 *Fuzzy Logic Designer*

When we test our system by experimenting through the rule table, we can see that the results we obtain are the same as the theoretically calculated results. This proves the accuracy of the result we obtained in ANFIS. When 3. and 8. lines are tried from our input data, the results and accuracy obtained are observed in the following ways as shown respectively in Fig.10 and Fig.11.

Table.2 *Data in line 3 in our entries*

β	β(rad)	$\eta^{(2)}$ =0.5	$\eta^{(2)}$ =0.3	$\eta^{(2)}$ =0.2	$\eta^{(2)}$ =0.05
10	0,1744	0,3909	0,2802	0,2457	0,147

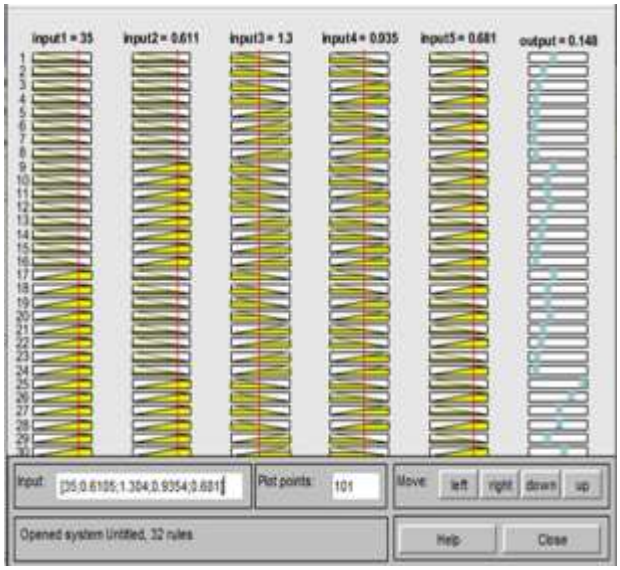

Figure.10 *Rule table that occurs when row 3 (table 2) is tried in the table where our input data is located*

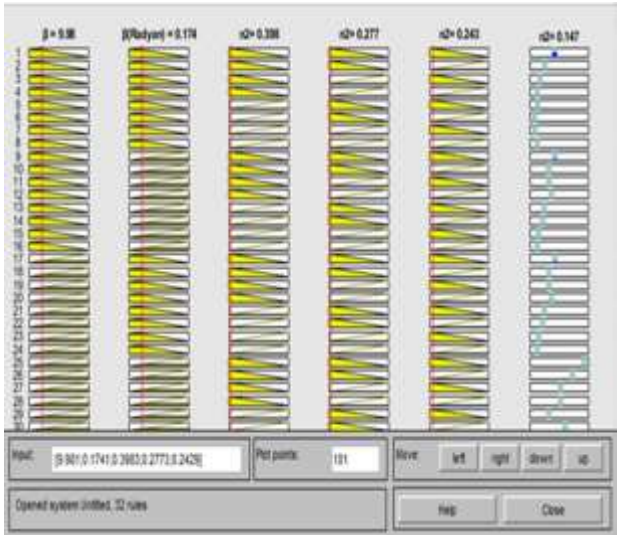

Figure.11 *Rule table that occurs when row 8 (table 3) is tried in the table where our input data is located*

Table.3 *Data in line 8 in our entries*

β	β(rad)	$\eta^{(2)}$ =0.5	$\eta^{(2)}$ =0.3	$\eta^{(2)}$ =0.2	$\eta^{(2)}$ =0.05
35	0,6105	1,304	0,9354	0,681	0,148

The ANFIS model structure formed as a result of the training is seen in Fig.12. According to this shape, a clear result is obtained by training 5 data inputs according to the rules.

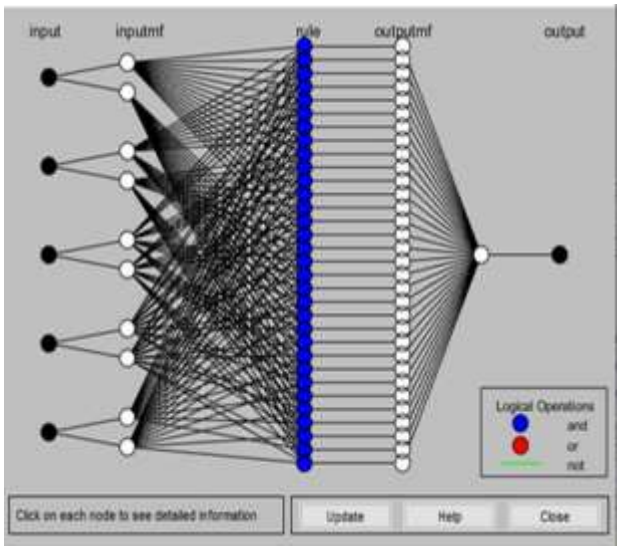

Figure.12 *Anfis Model Structure formed as a result of training*

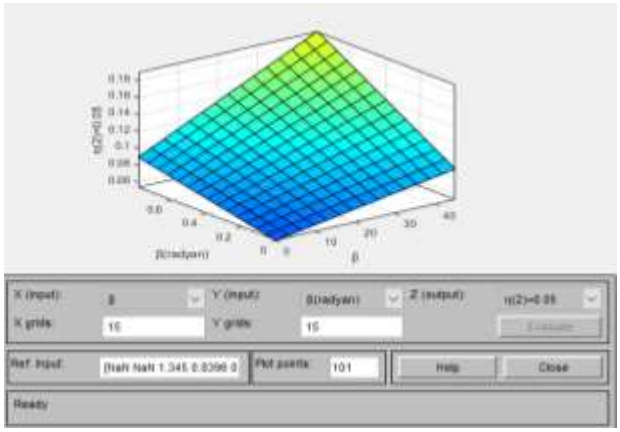

Figure.13 *Surface formed as a result of training*

5. Conclusions

The results of the simulation obtained were observed to be in harmony with the results obtained as a result of theoretical calculations. Thus, results were obtained by ANFIS method, which has a hybrid algorithm from artificial intelligence methods to predict the Theoretical Fracture Criteria

of Layered Elastic Composite Material. At the same time, predictions were obtained for different situations. Accordingly, we can explain the results as follows. The data obtained as a result of training with ANFIS were found to be exactly the same as the theoretical results in Fig.13. As a result of training with ANFIS, the error value in the training phase of the system is 4.0119e-05. The RMSE error value obtained by testing the network is 4.0119e-05. Artificial intelligence algorithms to be selected in these and similar studies should be tested first with theoretical and experimental studies and their compliance should be shown and the prediction phase should be proceeded. Thus, the results will be obtained from more than one point of view and trust will be provided.

Our studies on obtaining the values that give the properties of the theoretically obtained composite materials by machine learning methods in artificial intelligence continue today. We think that the comparative results obtained in this study will be important in the future literature.

Author Statements:

- **Ethical approval:** The conducted research is not related to either human or animal use.
- **Conflict of interest:** The authors declare that they have no known competing financial interests or personal relationships that could have appeared to influence the work reported in this paper
- **Acknowledgement:** The authors declare that they have nobody or no-company to acknowledge.
- **Author contributions:** The authors declare that they have equal right on this paper.
- **Funding information:** The authors declare that there is no funding to be acknowledged.
- **Data availability statement:** The data that support the findings of this study are available on request from the corresponding author. The data are not publicly available due to privacy or ethical restrictions.

References

[1]N. Guz (1992). Micromechanics of composite materials: Focus on Ukrainian research, *Special Issue of Applied Mechanics Reviews.* 45:13-107.

[2]A.N. Guz, (1990). Mechanics of compressive failure of composite materials, *Kiev: Nauk Dumka*,

[3]A.N. Guz, (1969). On the determination of the theoretical strength limit in compression of reinforced materials, *Dokl. Akad Nauk USSR Ser A* , 3:236-238 (in Russian).

[4]A.E. Green, R.S. Rivlin, R.T. Shield, (1952) General Theory of small elastic deformations superposed on finite elastic deformations, *ProcRoySoc Ser A* 211 (1104): 128-154.

[5]M.A. Biot, (1965). Mechanics of incremental deformations, New York: Wiley

[6]S.D. Akbarov, T. Sisman, N. Yahnioglu (1997). On the fracture of the unidirectional composites in compression, *Int. J. Eng. Sci.* 35:1115-1136. doi:10.1016/s0020-7225(97)00020-7

[7]S.D. Akbarov, A. Cilli, A.N. Guz. (199). The theoretical strength limit in compression of viscoelastic layered composite materials, *Composites Part B: Engineering*. 30:465-472. doi:10.1016/s1359-8368(99)00016-5

[8]A. Cilli, (1998). The fracture problems in compression of unidirectional fibre-layered composite materials, Doctoral Thesis, YTU, Istanbul

[9]S.D. Akbarov, A.N. Guz, (2002). Mechanics of curved composites, *Int. Appl. Mechanics*, 38: 1415-1439. doi.org/10.1023/A:1023253623082

[10]A.Cilli, (2011). On the theoretical strength limit of the layered elastic and viscoelastic composites in compression. *Applied Mathematical Modelling*, 35:5470-5479. doi.org/10.1016/j.apm.2011.04.032

[11]A. Çilli, (2016). Theoretical Fracture Criterion of the Layered Elastic Composite Materials *AIP Conference Proceedings*, 1722:1-4, doi.org/10.1063/1.4944270

[12]M. F. Keskenler, & E. F. Keskenler (2017) Bulanık Mantığın Tarihi Gelişimi. *Takvim-i* Vekayi, *5*(1):1-10.

[13]Harita ve Kadastro Mühendisleri Odası. "bulanik_mantik.htm". (10.06.2003) http://www.hkmo.org.tr/yayin/odadergi/s87/

[14]J. Yen, R. Langari, L. Zadeh, (1995). Industrial Applications of Fuzzy Logic and Intelligent Systems", *IEEE Press*, New York,

[15]G. Chen, T.T. Pham, (2020). Introduction to Fuzzy Sets, Fuzzy Logic, and Fuzzy Control Systems", *CRC Press*, Boca Raton London New York Washington, D.C

[16]S. Özmen-akyol ve E. Gülbandılar (2020). İris Çiçeği Türünün YSA Yöntemleri ve ANFIS ile Tahmini. *Eskişehir Türk Dünyası Uygulama ve Araştırma Merkezi Bilişim Dergisi*, 1(1):5-11

[17]J.-S. Jang, (1993). ANFIS: Adaptive network-based fuzzy inference systems. *IEEE Trans. Syst. Man. Cybern.*, 23(3):665–685 DOI: 10.1109/21.256541

[18]J. S. R. Jang, C. T. Sun, and E. Mizutani, (1997). Neuro Fuzzy and Soft Computing-A Computational Approach to Learning and Machine Intelligence [Book Review], "*IEEE Trans. Automat. Contr.*, 42(10):1482–1484

[19]P. Perez, (2001). Prediction of sulfur dioxide concentrations at a site near downtown Santiago, Chile, *Atmos. Environ.*, 35(29):4929–4935 doi.org/10.1016/S1352-2310(01)00268-0

[20]J. S, Abduljabar, (2011). Bulanik Mantik Yöntemler Kullanılarak Gazlı İçeceklerde Karbondioksit

Kontrolü, Ankara Üniversitesi Fen Bilimleri Enstitüsü, Yüksek Lisans Tezi, Ankara

[21]Y. Özcanlı, F. Kosovalı Çavuş, M. Beken (2016). Comparison of Mechanical Properties and Artificial Neural Networks Modeling of PP PET Blends. *Acta Physica Polonica A*, 130(1): 444-446. Doi:10.12693/APhysPolA.130.444

International Journal of Computational and Experimental Science and ENgineering (IJCESEN)
Vol. 8-No.2 (2022) pp. 40-48
http://dergipark.org.tr/pub/en/ijcesen

ISSN: 2149-9144

Research Article

Eikonal Approximation for K^+–Nucleus Elastic Scattering

Nagat A. ELMAHDY[1]*, Haytham GAMAL[2]

[1] Basic Science Department, Modern Academy for Engineering and Technology, Cairo, Egypt
* **Corresponding Author Email** : nagat_elmahdy@yahoo.com **ORCID:** 0000-0002-6152-5842

[2]Electronics Engin.and Communication Technology Dep. Modern Academy for Engin.and Technology, Cairo, Egypt
Email : haytham_gamal8@hotmail.com **ORCID:**0000-0003-0880-2011

Article Info:

DOI: 10.22399/ijcesen.1079685
Received : 27 February 2022
Accepted : 14 April 2022

Keywords

Equivalent local potential
Eikonal approximation
Kaon elastic scattering cross section
Scattering amplitudes parameters
Nuclear density distributions

Abstract:

The elastic scattering of kaons from different targets ^{6}Li, ^{12}C, and ^{40}Ca at energies 635, 715, and 800 MeV have been studied. The equivalent local potential form of Kisslinger optical potential with the eikonal approximation using Wallace expansion up to the 2nd order have been used. The potential depends on the density of the target nuclei, and the scattering amplitude parameters. Satisfactory fits to the elastic scattering experimental data are obtained.

1. Introduction

It is known that the K^+ meson scattering can be used as a weak hadronic interacting probe for investigating the neutron density distributions in nuclei which is providing insights into the nature of the scattering. Therefore the experimental data on elastic differential cross sections at intermediate energies [1,2] are under the permanent attention of theoreticians for years. Many optical model analyses of the elastic scattering of kaons from nuclei have been carried out using potentials of the Kisslinger form [3], its local equivalent form is introduced by Johnson [4], microscopic optical potential [5], and other forms for different nuclear density models.

The first and second-order corrections to the zero order eikonal phase shifts for heavy-ion elastic scattering based on the Coulomb trajectories of colliding nuclei have been applied satisfactory and improve the agreement with the exprimental data [6]. Also this work extended to cover the charged pions scattering on nuclei by using the Coulomb modified eikonal phase shift and its first order correction [7]. It has been applied satisfactory to 800 MeV/c pions scattering from ^{12}C and ^{40}Ca nuclei. The overall results are in excellent agreement at momentum 800 MeV/c and the agreement extended to the angle 36^o. The local form of the Kisslinger optical potential succeeded before with the eikonal approximation model in analysis of pion scattering without recourse to the complexities of the nonlocal interactions [8,9].

Among all the hadronic probes, K^+ meson holds special properties, below 1 GeV/c, the K^+-N strong interaction has a slow energy and momentum dependence and it is the weakest of all strong-interaction processes [10].

Because of the quark content of the K^+ which can't annihilate with valence quark content of the nucleon, K^+ has a long mean free path in the nuclear matter and capable of probing the interior of nuclei. A small cross section means a long mean free path $\left(\lambda = \frac{1}{\rho\sigma} > 5fm\right)$ for propagation of the K^+ in the nuclear medium, in contrast to the strongly interacting particles which get absorbed at the surface [11], so it is an ideal probe to study nuclear structure, and for a light nucleus, such as ^{12}C, the uncertainties which appear in working with the strong interaction are much smaller [12].

Recently, Ebrahim [10] proposed that the equivalent local optical potential with the zero-range distorted-wave Born approximation can be used to analyze the K^+-nucleus elastic scattering but needs an enhancement in the dominated S11 K^+-N phase shift by 10 % for ^{6}Li and around 12 % for ^{12}C, and ^{40}Ca nuclei. The DWUCK4 code is used to calculate the angular distributions with distorted-wave Born approximation. The charge distribution is used for ^{6}Li, the harmonic oscillator form for ^{2}H and ^{12}C, and the three parameter Fermi 3PF shape distribution of nucleons is used for ^{40}Ca.

The Ericson-Ericson Lorentz-Lorentz (EELL) parameter ζ slightly affects the elastic scattering. The disagreement between the calculated results and data at K^+-^{12}C is about 15% at 800 MeV/c but appears to decrease with decreasing momenta [10]. A good agreement by using the 3PF distribution density for the ^{40}Ca at 800 MeV/c and the polarization $\zeta = 1.0$ is obtained by increasing the S11 phase shift by 12%. If the K^+-N phase shifts increase the nucleon size will increase; a ''swelling'' of the nucleon in the nuclear medium. This means that the K^+-N interaction inside a nucleus will differ from the free space. The local optical potential can serve as a reliable model for kaon-nucleus scattering.

Lukyanov [5] used the derived microscopic optical potential in calculation of the differential elastic-scattering cross sections for the interaction of K^+ mesons with ^{12}C and ^{40}Ca nuclei at energies 635, 715, and 800 MeV. It is determined by the amplitude for kaon–nucleon scattering and the density distribution of point like nucleons of the target nucleus. The results obtained by calculating optical potentials depend on the density distributions of point like neutrons and protons in the ground state of the nucleus. It turns out that, in this model, there is no need for including nonlocal terms in the potential, in contrast to what is done in the Kisslinger model, or for employing phenomenological optical-model potentials involving a large number of free parameters.

Originally, the eikonal approximation has taken a considerable attention after the work of Glauber [13] who obtained a Fourier-Bessel representation of the scattering amplitude which justified for all angles on general grounds of analyticity in the momentum transfer. Glauber extended it by using a frozen target approximation to convert the many body scattering problem into a potential scattering problem in which the potential depends on the coordinates of the target.Wallace [14] proposed a sequence of four approximations to the exact impact parameter of the scatterin matrix. In eikonal propagation picture, the accelerated projectile propagates through a frozen target without changing its transverse position but picking up an eikonal phase [15].

The present study of the K^+ scattering is focused on eikonal approximation with its first and second corrections. This interest has been particularly motivated by a hope to explain well the K^+-nucleus elastic scattering data. We give a simple physical description to the quantum mechanical formulation of the eikonal propagation which has been extensively used in hadronic interaction problems in dense (nuclear) environment at high energy. This is illustrated that by calculating the differential cross sections with the first and second order eikonal corrections [15]. For the first time the local potential of Johnson and Satchler [4], together with the eikonal approximation with 2nd order corrections were used to analyze the angular distributions of elastically scattered K^+ from ^{6}Li, ^{12}C, and ^{40}Ca at kaon lab momenta ranging from 635-800 MeV/c. Satisfactory agreement with the measured angular distributions and the local optical potential calculation is obtained at forward angles. MATLAB CODE is used for all calculations and formulas. The present work is precisely an attempt to understand the range of validity and limits of the applicability of the eikonal approximation by using local Kisslinger optical potential. In Sec.II the basic formulas of the potential equations and an explicit quantum mechanical description of the eikonal approximation are given. Sec. III is devoted to the results and discussions followed by conclusion in Sec. IV.

2. Formalism

Meson-nucleus elastic scattering data are analyzed using an optical potential of the Kisslinger form [3]. By using the Krell-Ericson transformation [16] and solving of the Klein-Gordon equation. The basic equation of the phenomenological local optical potential will be

$$U(r) = \frac{(\hbar c)^2}{2\omega}\left(\frac{q(r)}{1-\alpha(r)} - \frac{k^2\alpha(r)}{1-\alpha(r)} - \left(\frac{\frac{1}{2}\nabla^2\alpha(r)}{1-\alpha(r)} + \left(\frac{\frac{1}{2}\nabla\alpha(r)}{1-\alpha(r)}\right)^2\right)\right) + \frac{\alpha(r)V_c - \left(\frac{V_c^2}{2\omega}\right)}{1-\alpha(r)} \qquad (1)$$

which introduced as potential without sharp edge. The quantities $q(r)$ and $\alpha(r)$ can be expressed in terms of meson-nucleon scattering amplitudes and the target nucleus density distributions with their

gradients. The quantities $q(r)$ and $\alpha(r)$ are complex quantities depend on energy and target densities (proton and neutron densities). They defined as fellows

$$q(r) = q_0(r) + \Delta q(r) \qquad (2)$$

$$\alpha(r) = \frac{\alpha_1(r)}{1+\frac{1}{3}\zeta\alpha_1(r)} + \alpha_2(r) \qquad (3)$$

where, $q_0(r) = -4\pi p_1\left(b_0\rho(r) - b_1\Delta\rho(r)\right)$ (4)

$$\Delta q(r) = -\frac{1}{2}\varepsilon\nabla^2\left(\alpha_1(r) + \frac{1}{2}\alpha_2(r)\right) \qquad (5)$$

$$\alpha_1 = 4\pi\frac{\left(c_\circ\rho(r) - c_1\Delta\rho(r)\right)}{1+(\omega/Mc^2)} \qquad (6)$$

$$\alpha_2 = 4\pi\frac{\left(C_\circ\rho_{np}(r) - C_1\rho(r)\Delta\rho(r)\right)}{1+(\omega/2\,Mc^2)} \qquad (7)$$

and

$$\rho(r) = \rho_n(r) + \rho_p(\mathrm{r}) \qquad (8)$$

$$\Delta\rho(r) = \rho_n(r) - \rho_p(\mathrm{r}) \qquad (9)$$

$$\rho_{np}(r) = 4\rho_n(r)\rho_p(r) \qquad (10)$$

where $\rho_p(r)$ and $\rho_n(r)$ are proton and neutron density distributions of target nucleus, respectively. We use p_1 and p_2 as kinematic constants which depend on meson energy. M is the mass of a nucleon and ω is the total energy of meson in the centre of mass [17]. ζ is the Ericson-Ericson Lorentz-Lorentz (EELL) parameter which parameterizes the polarization of the nuclear medium [18]. The ζ parameter isn't exactly known because its determination requires taking into account all the effects together which make the calculation unreliable [19]. This parameter has a small effect above the Δ-resonance in the calculations compared to its effect in the resonance energy. The quantities bi and ci $(i = 0,1)$ are referred to the first order amplitude parameters, while the complex amplitude second-order parameters Bi and Ci $(i = 0,1)$ describe the pion absorption. Different formulas of the radial density distribution for the considered nuclei are used. The formulas are the charge distribution density (CH), the harmonic oscillator (HO) model, the two parameter Fermi (2PF) model, and the three parameter Fermi (3PF) model, all are used to clarify the general changes in the radial variations of the density from one nucleus to another. CH density model gives information about the charge density and hence primarily about the proton distribution and it takes the form [10]

$$\rho_{ch}(r) = \frac{Z}{8\pi^{3/2}}\left[\frac{1}{a^3}\,exp\,\left(\frac{-r^2}{4a^2}\right) - \frac{c^2\left(6b^2-r^2\right)}{4b^7}\,exp\,\left(\frac{-r^2}{4b^2}\right)\right] \qquad (11)$$

where $a, and\ b$ are adjustable parameters, Z is the atomic number and extended to be taken for neutron density form, its domain of use for light nuclei and it will be named CH model. The Harmonic Oscillator (HO) is defined as [4]:

$$\rho(r) = \rho_o\left[1 + \alpha\left(\frac{r}{c}\right)^2\right]\exp\left[-\left(\frac{r}{c}\right)^2\right] \qquad (12)$$

where c is a parameter related to root mean square radius, α is the oscillator constant and ρ0 is the density of nuclear matter at r = 0. The two-parameter Fermi (2PF) is defined as [4]:

$$\rho_i(r) = \frac{\rho_{oi}}{1+\exp\left(\frac{r-c_i}{a_i}\right)} \qquad (13)$$

where $i = n\ or\ p$ for proton or neutron, and c is the half density radius, a is the diffuseness parameter (a measure of the thickness of the surface layer of nucleus) and ρ0 is the central density parameter.
The three-parameter Fermi (3PF) is defined as [18]:

$$\rho_i(r) = \frac{\rho_{oi}\left(1+\frac{\omega_i r^2}{c_i^2}\right)}{1+\exp\left(\frac{r-c_i}{a_i}\right)} \qquad (14)$$

where $i = n\ or\ p$ for proton or neutron respectively, and ci is the half density radius, a_i is the diffuseness, ρ0 is the central density parameter and ω_i is an adjustable parameter. All the density forms of neutrons and protons are subjected to the normalization condition:

$$\int \rho_i(\bar{r})\,d\bar{r} = (A - Z)\ or\ Z \qquad (15)$$

where Z is the atomic number of the nucleus and in particular it leads for 3PF and 2PF density models. The nuclear density is taken as

$$\rho(r) = \rho_n(r) + \rho_p(r) \qquad (16)$$

All the parameters of these three types of densities are listed in Table 1 and 2.

***Table 1**: The ground-state density distributions parameters and the densities of nuclear matter for the charged density, the harmonic oscillator, 2PF, and 3PF models (p for protons).*

Nucleus	Model	c_p	a_p	w_p	ρ_{0p}	Ref
^{6}Li	3PF	1.55	0.07	0.015	0.08	*
	2PF	2.063	0.096	0	0.08	*
^{12}C	3PF	2.002	0.5	0.2595	0.08	[20]
	2PF	2.5	0.37	0	0.075	[21]
^{40}Ca	3PF	3.68	0.546	-0.1	0.0743	[22]
	2PF	3.42	0.55	0	0.0951	[22]
Nucleus	**Model**	a	**b and** α	**C**	ρ_{0p}	**Ref**
^{6}Li	CH	0.928	1.26	0.48	0.51262	[10]
	HO	1.727	4.5		0.08994	*
^{12}C	CH	0.928	1.26	0.48	0.1538	*
	HO	1.516	2.234		0.0711	[10]
^{40}Ca	CH	0.928	1.26	0.48	0.51262	*
	HO	1.727	4.5		0.08994	*

* The values stated in all tables are satisfying the root mean square radius for each nucleus.

***Table 2**: The ground-state density distributions parameters and the densities of nuclear matter for the charged density, the harmonic oscillator, 2PF, and 3PF models (n for protons).*

Nucleus	Model	c_n	a_n	w_n	ρ_{0n}	Ref
^{6}Li	3PF	1.55	0.07	0.015	0.08	*
	2PF	2.063	0.096	0	0.08	*
^{12}C	3PF	2.002	0.5	0.2595	0.08	[20]
	2PF	2.5	0.37	0	0.075	[21]
^{40}Ca	3PF	3.97	0.42	-0.1	0.0743	[22]
	2PF	3.42	0.55	0	0.0951	[22]
Nucleus	**Model**				ρ_{0n}	**Ref**
^{6}Li	CH				0.51262	[10]
	HO				0.08994	*
^{12}C	CH				0.15380	*
	HO				0.0711	[10]
^{40}Ca	CH				0.51262	*
	HO				0.08994	*

* The values stated in all tables are satisfying the root mean square radius for each nucleus.

According to Wallace, the expansion of the phase shift function $\chi(b)$, as a power series in the strength of the scattering potential and its derivatives [6]

$$\chi_i(b) = \sum_{n=0}^{j} \chi^{(n)}(b) \quad (18)$$

where

$$\chi^{(n)}(b) = -\frac{k[\mu/(\hbar k)^2]}{(n+1)!\, b^{2n}} \left[b^2\left(1 + b\frac{d}{db}\right)\right]^n \int_0^\infty U^{n+1}\left[(b^2 + z^2)^{1/2}\right] dz \quad (19)$$

The zero order term in Eqn. (19) gives the eikonal phase shift

$$\chi^{(0)}(b) = -\frac{\mu}{\hbar^2 k}\int_0^\infty U\left((b^2 + z^2)^{\frac{1}{2}}\right) dz \quad (20)$$

For local potential the first and second order corrections are given, respectively, by

$$\chi^{(1)}(b) = -\frac{\mu^2}{2\hbar^4 k^3}\left(1 + b\frac{d}{db}\right)\int_0^\infty U^2\left((b^2 + z^2)^{\frac{1}{2}}\right) dz \quad (21)$$

$$\chi^{(2)}(b) = -\frac{\mu^3}{6\hbar^6 k^5}\left(3 + 5b\frac{d}{db} + b^2\frac{d^2}{db^2}\right)\int_0^\infty U^3\left((b^2 + z^2)^{\frac{1}{2}}\right) dz \quad (22)$$

where U is the optical potential, b is the impact parameter, μ is the reduced mass, and k is momentum in the centre of mass system. The S matrix is expressed as

$$S_l = \exp(2i\delta_l), \quad and \quad \delta_l = \frac{1}{2}\chi(b) \quad (23)$$

The general expression for the elastic scattering amplitude between the spin 0 kaon and the target nucleus is given by

$$f(\theta) = f_c(\theta) + (2ik)^{-1}\sum_i (2l+1)\exp(2i\eta_l)\,(S_l - 1)\,P_l(\cos\theta) \quad (24)$$

where $f_c(\theta)$ is the Coulomb scattering amplitude, k is the centre of mass momentum, and η_l is the Coulomb phase shift [23]. The differential cross section is given by

$$\frac{d\sigma}{d\Omega} = |f(\theta, \Omega)|^2 \quad (25)$$

3. Results and Discussion

A. The Eikonal Phase Shift with Wallace corrections

The eikonal phase shifts with Wallace corrections up to 2nd order have been used to calculate the elastic scattering differential cross section of K^+-nucleus as shown in figures (1-3). All these calculations have been done for $\zeta = 1$ (the polarization parameter). Fig. 1 shows with the reaction K^+-^{6}Li at energy 715 MeV using 2PF nuclear density model. Fig. 2 shows with the reaction K^+-^{12}C at a) energy 635 MeV using CH nuclear density model, b) at energy 715 MeV using HO model for the target density. From what proceeds, it can be seen that calculation with different corrections up to 2nd order of the eikonal expansion has no effect on the calculated elastic scattering differential cross section. The Figures 1-2 show no effect of higher order corrections on the results of the elastic cross section, since the relatively small kaon mass to its momentum ratio, converges the eikonal expansion rapidly. The eikonal phase shift corrected up to second order term is calculated using the same scattering amplitude parameters of Ebrahim [24,25]. Figures 3 shows the calculations of the elastic scattering differential cross section of K^+-nucleus depending on these parameters for the reactions $K^+ + {}^{6}$Li at energy 715 MeV, and $K^+ + {}^{12}$C at energy 635 MeV. It presents that the result doesn't agree well with the experimental data although it comes close for lower target masses and incident energies. The

eikonal model didn't come very well with these taken amplitude parameters [24,25]. Such approach with previously used scattering amplitude parameters didn't fit properly the data and eventually get a limited success. In the case of the eikonal approach, since the parameters of the scattering amplitudes are based on the free kaon-nucleon scattering. This keeping structural frame of the scattering amplitudes to get the best possible values to fit different targets and energies with different models of nuclear densities to obtain the best possible fit with the eikonal approach for scattering. The resulting best fit scattering amplitude parameters used in the present work for K+- nucleus are shown in Tables 3, 4, and 5. The difference in the two approximations, the partial wave impulse approximation, in which the binding forces are ignored during collision, and the eikonal approximations sticks to the straight line path as a

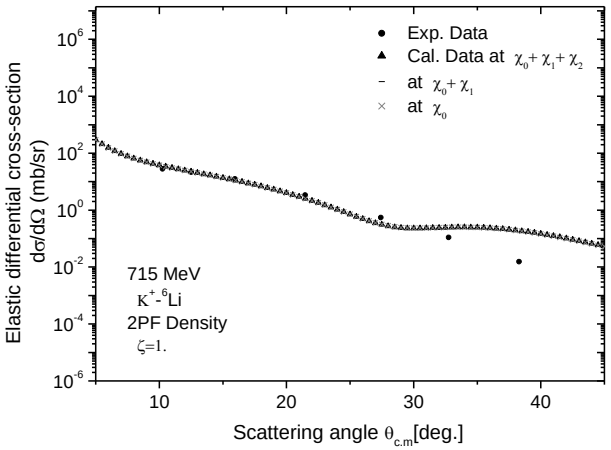

Figure 1. *The elastic scattering cross sections for K^+ + 6Li with 2PF density model by using the zero, first and the second-order terms of the eikonal phase shifts at 715 MeV. The experimental data is taken from Ref.[26].*

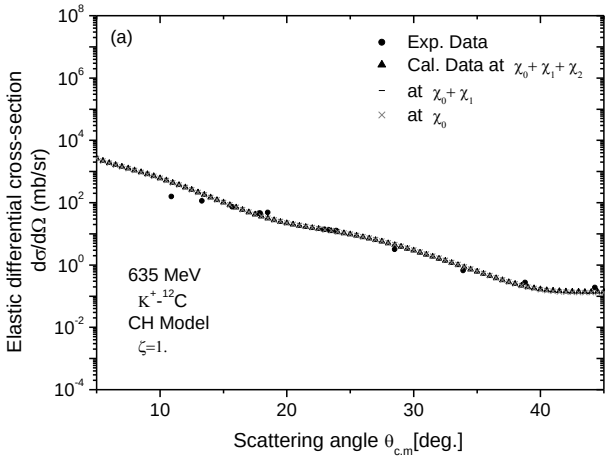

Figure 2. *The elastic scattering cross sections for K^+ + 12C using the zero, first and the second-order terms of the eikonal phase shifts (a) CH model at 635 MeV, (b) HO model at 715 MeV. The experimental data is taken from Ref.[26].*

Table 3*: First-order amplitude parameters used in the present work with K+ as a projectile and (6Li ,40Ca) as targets. Note: in each case the upper row is the real part and the lower row is the imaginary part for each target.*

	^{6}Li	^{40}Ca
T_π (MeV)	715	800
k (fm^{-1})	4.66	5.86
p_1	2.11	2.34
p_2	1.56	1.67
b_0 (fm)	0.07892	2.0165
	0.034847	1.121890
b_1 (fm)	0.03622	0.03567
	0.1155600	0.0353200
c_0 (fm^3)	0.005949	-0.05047
	0.1153390	0.090000
c_1 (fm^3)	0.01502	0.01352
	-0.0447327	0.0143100

Table 4*: First-order amplitude parameters used in the present work with K+ as a projectile and 12C as target. Note: in each case the upper row is the real part and the lower row is the imaginary part for each target.*

	^{12}C	^{12}C	^{12}C
T_π (MeV)	635	715	800
k (fm^{-1})	4.688	5.066	5.456
p_1	2.12	2.2	2.26
p_2	1.56	1.6	1.63
b_0 (fm)	2.232501	2.3658	2.116427
	1.021470	2.648000	-0.167816
b_1 (fm)	0.026355	-0.0593	0.033963
	-0.041603	0.0536000	0.0648988
c_0 (fm^3)	-0.09629	0.00212	-0.051
	0.1937890	0.1673000	0.3724900
c_1 (fm^3)	-0.03406	0.006173	-0.01464
	-0.0144586	-0.0491000	0.0008428

Table 5*: Second-order amplitude parameters used in the present work with K+ as a projectile. Note: in each case the upper row is the real part and the lower row is the imaginary part for each target.*

	^{6}Li	^{12}C	^{12}C	^{12}C	^{40}Ca
T_π (MeV)	715	635	715	800	800
C_0 (fm^3)	0	0	0	-2.8	-3.6
	0	0	0	-3.6	1.0
C_1 (fm^3)	0	0	0	0	0
	0	0	0	0	0

special direction which makes a stringent semiclassical limit. These conceptual differences reflect on the different values of the amplitude parameters for fitting the experimental data at each method. So, with eikonal model, it is possible to get the agreement with data only with the variation of the amplitude parameters freely and isn't possible to get it with previously calculated parameters. This makes the problem more complicated and pushes the way to find The difference in the two approximations, the partial wave impulse approximation, in which the binding forces are ignored during collision, and the eikonal approximations sticks to the straight line path as a

special direction which makes a stringent semiclassical limit. These conceptual differences reflect on the different values of the amplitude parameters for fitting the experimental data at each method. So, with eikonal model, it is possible to get the agreement with data only with the variation of the amplitude parameters freely and isn't possible to get it with previously calculated parameters. This makes the problem more complicated and pushes the way to find a more systematic way to the correlation between the scattering amplitudes calculated before and those obtained at best possible fit.

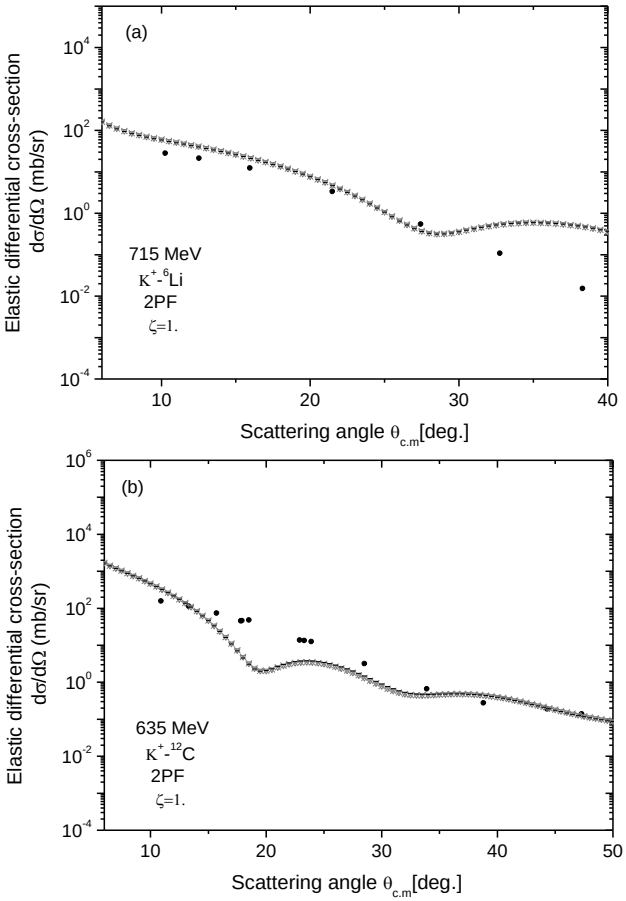

Figure 3. *The elastic scattering cross sections (a) for $K^+ + 6Li$ with 2PF density model at 715, (b) for $K^+ + 12C$ with 2PF density model at 635 MeV. The scattering amplitude parameters are from Ref.[24,25]. The experimental data is taken from Ref.[26].*

B. Effect of the target density model

The local potential terms depend on the target nuclear density distribution. To study this factor, four different models of the nuclear densities which describe the shape of the target nucleus, all are used to clarify the general changes in the radial variations of the density from one nucleus to another. The values of $\zeta = 1$, has been used in all calculations. The fitted scattering amplitude parameters of Table 2 have been used in all the following calculations of the elastic scattering differential cross section of K+-nucleus.

K+-^{6}Li: Figures (4-5) show our calculation of K+-6Li using different types of target density model (CH, HO, 2PF, 3PF) compared with experimental data.

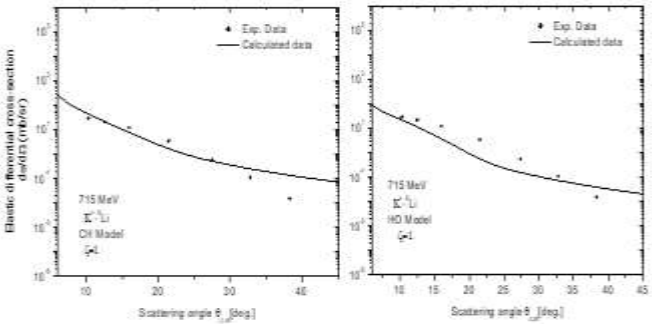

Figure 4. *The elastic scattering of $K^+ + 6Li$ by using CH and HO density model with ζ=1 at energy 715 MeV. The experimental data is taken from Ref.[26].*

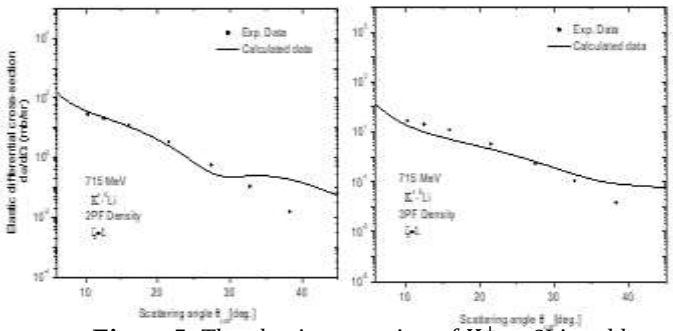

Figure 5. *The elastic scattering of $K^+ + 6Li$ and by using 2PF and 3PF density model with ζ=1 at energy 715 MeV. The experimental data is taken from Ref.[26].*

Clearly, the best fitting obtained among the target's densities is the 2PF model with the eikonal approach. The core density plays an important part at large scattering angles.

K+-^{12}C: Similarly, by applying calculation of K+-12C using different types of target density model (CH, HO, 2PF, 3PF), it is found the 2PF and 3PF models of density have limited agreement and produce a minimum moves to smaller angles with increasing the energy. The best fitting obtained among the target's densities is the CH model with the eikonal approach as shown in Figure (6).

K+-^{40}Ca: Figure (7) shows our calculation of K+-40Ca using different types of target density model (2PF, 3PF) compared with the experimental data. The 2PF and 3PF distributions are shown for 40Ca. These two models have been only used because the

CH and HO failed to describe the heavier nuclei. It could be seen that the calculations with the 2PF model for the density of the target nucleus 40Ca gives the best results at small angles as shown in figures. The following Table 6 shows all the best density models with each target and energy, which summaries the present work results of K+ with ^{6}Li, ^{12}C, and ^{40}Ca

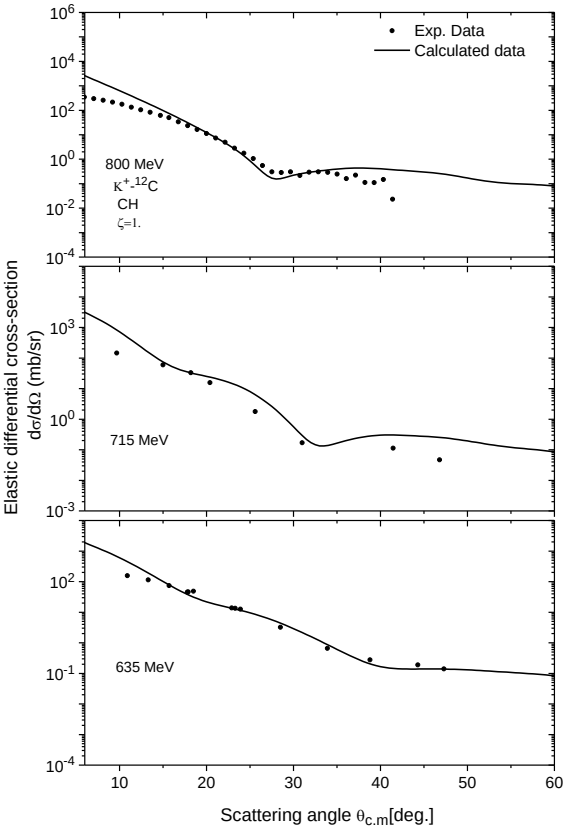

Figure 6. *The elastic scattering of $K^{+} + 12C$ by using CH density model with ζ=1 at energies; 635 MeV, 715 MeV, and 800 MeV. The experimental data is taken from Ref.[26,27].*

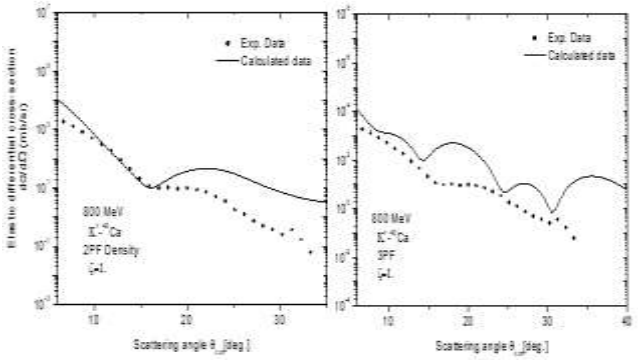

Figure 7. *The elastic scattering of $K^{+} + 40Ca$ by using 2PF and 3PF density model with ζ=1 at energy 800 MeV. The experimental data is taken from Ref.[26].*

Table 6*: the scattering angle range of agreement for the elastic differential cross sections of K+ with different targets with their best density model at different energies.*

Projectile	Energy (MeV)	Target	Best Density Model	Agreement Range
K^{+}	715	^{6}Li	2PF	10º to 33º
	635	^{12}C	CH	10º to 50º
	715	^{12}C	CH	10º to 40º
	800	^{12}C	HO	10º to 30º
	800	^{40}Ca	2PF	10º to 15º

4. Conclusion

We have studied the angular distributions of the elastic scattering differential cross sections for K+ on 6Li, 12C, and 40Ca at energies 635, 715, and 800 MeV. Where we show how well the eikonal approximation model and local form of Kisslinger were able to reproduce the experimental data. To this purpose we have used the eikonal model by considering the first and the second-order correction terms to the eikonal phase shifts. Also, the local Kisslinger optical potential depends on different sets of free adjustable parameters; the type of density model, the amplitude parameters, and the EELL parameters. It seems clear that a full analysis of these parameters will be required if a detailed comparison is to be made with the experimental results. The accuracy of the agreement with experimental data can be improved by changing these parameters to reach the best fit.

The higher order corrections would clarify the relationship between the eikonal expansion and the impact parameter b. Corrections, which are incorporated to the eikonal expansion, have nearly no effect on the results because of the massive projectile and its large momentum. The correlation parameter ζ parameterizes the polarization of the nuclear medium.

The availability of change the EELL parameter gave nearly no change on the calculated elastic scattering cross sections in the experimental range of angles. In order to check for possible density-dependent effects, the four sets of density models are applied. For the nuclear density distributions, it was assumed that the proton and neutron densities were similar. From the comparison with the experimental data, the 2PF model of density gives satisfactory results with the most cases of interactions. The CH model of nuclear density predictions was suitable with 12C and the 2PF nuclear density model predicted well the calculated results for 6Li and 40Ca. 3PF model was the worst in most cases of study.

In deriving the amplitudes parameters, it is necessary to transform the kaon-nucleon scattering amplitude from the two-body centre of mass system to the kaon-nucleus centre of mass system. The most significant difference between the free nucleon cases and fitted parameters are that the fitted magnitude of Re (bo), Im (bo), Re (co), and Im (co). In addition, adding values for the second-order amplitudes parameters Re (Co) contributes to give the best fitting. The present elastic scattering data can be well reproduced by local form of Kisslinger potential with adjustable parameters which rather different than the free kaon-nucleon values. We note that the regularization of the local Kisslinger optical potential used in this work by the introduction of the fitting parameters can serve as a tool to obtain a best agreement with the experimental data.

After having made an adjustment of the potential parameters, and using the suitable model of density, we have deduced a set of potential parameters which describe the elastic scattering cross sections for nuclei under examination. It is found also that the effective potential parameters slightly change from nucleus to nucleus.

The local Kisslinger model with the eikonal model was found to be successful for all types of interactions in the present work. The close agreement between theory and experiment is mainly for the forward angles less than 40o and in fair agreement with $40^o < \theta < 50^o$. As a whole the eikonal model description is quite successful as a framework for a description of K+- nucleus scattering. In addition to being a study of the eikonal model, this work also provided a systematic and comprehensive local Kisslinger potential model analysis of mesons-nucleus scattering. The calculated cross sections reproduced the experimental data quite well for the considered nuclei.

Author Statements:

- **Ethical approval:** The conducted research is not related to either human or animal use.
- **Conflict of interest:** The authors declare that they have no known competing financial interests or personal relationships that could have appeared to influence the work reported in this paper
- **Acknowledgement:** The authors declare that they have nobody or no-company to acknowledge.
- **Author contributions:** The authors declare that they have equal right on this paper.
- **Funding information:** The authors declare that there is no funding to be acknowledged.
- **Data availability statement:** The data that support the findings of this study are available on request from the corresponding author. The data are not publicly available due to privacy or ethical restrictions.

References

[1] D. Marlow, P. D. Barnes, N. J. Colella, S. A. Dytman, R. A. Eisenstein, R. Grace, F. Takeutchi, W. R. Wharton, S. Bart, D. Hancock, R. Hackenberg, E. Hungerford, W. Mayes, L. Pinsky, T. Williams, R. Chrien, H. Palevsky, and R. Sutter (1982) Kaon scattering from C and Ca at 800 MeV/c". *Phys. Rev. C* 25: 2619.

[2] R.E.Chrien, R.Sawafta, R.J.Peterson, R.A.Michael, and E.V.Hungerford. (1997) Elastic and Inelastic Scattering of K+ from ^{6}Li and ^{12}C. *Nucl. Phys. A* 625: 251. DOI: 10.1016/S0375-9474(97)00384-9

[3] L. S. Kisslinger. (1955) Scattering of Mesons by Light Nuclei *Phys. Rev*. 98:761. DOI:https://doi.org/10.1103/PhysRev.98.761

[4] M. B. Johnson and G. R. Satchler. (1996) Characteristics of local pion-nucleus potentials that are equivalent to Kisslinger-type potentials. *Ann. Phys., NY* 248:134.

[5] V. K. Lukyanov, E. V. Zemlyanaya, K. V. Lukyanov, D. N. Kadrev, A. N. Antonov, M. K. Gaidarov, and S. E. Massen(2009) Calculations of 8He+p Elastic Cross Sections Using Microscopic Optical Potential. *Arxiv:* 0908.1008 V1 [nucl. th].

[6] Moon Hoe Cha, and Yong Joo Kim. (1995) Higher-order corrections to the eikonal phase shifts for heavy-ion elastic collision. *Phys. Rev. C* 5:212-216. DOI:https://doi.org/10.1103/PhysRevC.51.212

[7] Moon Hoe Cha, and Yong Joo Kim. (1996) First-order eikonal approximation for the elastic scattering of 800 MeV/c pions from ^{12}C and ^{40}Ca nuclei *Phys. Rev. C* 54:429. DOI: 10.1103/PhysRevC.54.429

[8] M. B. Johnson (1980) Analytical theory of pion single and double charge exchange in resonance region. I. Geometrical limit. *Phys. Rev. C* 22:192. DOI:https://doi.org/10.1103/PhysRevC.22.192

[9] M. B. Johnson and E. R. Siciliano. (1983) Isospin dependence of second order pion nucleus optical potential. *Phys. Rev. C* 27:730-750. DOI:https://doi.org/10.1103/PhysRevC.27.730

[10] A. A. Ebrahim and S. A. E. Khallaf. (2002) Elastic and inelastic scattering of K+ from nuclei *Phys. Rev. C* 66:044614. DOI: DOI: https://doi.org/10.1103/PhysRevC.66.044614

[11] R. Weiss, J. Aclander, J. Alster, M. Barakat, S. Bart, R. E. Chrien, R.A. Krauss, K. Johnston, L Mardor, Y. Mardor, S. May Tal-beck, E. Piasetzky, P. H. Pile, R. Sawafta, H. Seyfarth, R. L. Stearns, R.J.

Sutter and A.I. Yavin. (1994) Measurement of low energy K+ total cross sections on N=Z nuclei *Phys. Rev. C*49: 2569.

[12] R. Micheal, M. Barakat, S. Bart, R. E. Chrien, D. J. Ernest, S. Hama, K. H. Hicks, Wendy Hinton, E. V. Hungerford, M. F. Jiang, T. Kishimoto, C. M. Kormanyos, L. J. Kurth, L. Lee, B. Mayes, R. J. Peterson, L. Pinsky, R. Sawafta, R. Sutter, L. Tang, and J. E. Wise. (1996) K+ elastic scattering from C and Li-6 at 715-MeV/c. *Phys. Lett. B* 382:29-34.

[13] R. J. Glauber. (1959) High-Energy Collision Theory, edited by W. E. Britten Interscience, *New York.*

[14] S. J. Wallace. (1973) Eikonal expansion" *Ann. of Phys.* 78:190-257. DOI: https://doi.org/10.1016/0003-4916(73)90008-0

[15] Alex Kover, and Urs Achim Weidemann. (2001) Eikonal evolution and gluon radiation. *Phys. Rev. D*64:114002.

[16] M. Krell and T. E. O. Ericson (1969) Energy levels and wave functions of pionic atoms. *Nucl. Phys. B* 11:521-550. DOI: https://doi.org/10.1016/0550-3213(69)90301-0

[17] Reza Safari. (2006) A new pion-nucleus optical potential valid for Δ-resonance region. *International Journal of Pure and Applied Mathematic*s. 29(2):141-151.

[18] S.A.E. Khallaf and A.A. Ebrahim. (2000) Analysis of π±-nucleus elastic scattering using a local potential. *Phys. Rev. C* 62:024603. DOI:https://doi.org/10.1103/PhysRevC.62.024603

[19] Ricardo Ignacio AIvaIez del Castillo, (1991) Ph.D. Thesis, *McGill University Montreal*, Canada,

[20] R. Alvarez del Castillo and N. B. de Takacsy (1991) Analysis of low energy π+ scattering to second O+ states. *Phys. Rev. C* 43:1389. DOI:https://doi.org/10.1103/PhysRevC.43.1389

[21] B. M. Preedom, S. H. Dam, C. W. Darden, III, R. D. Edge, D. J. Malbrough, T. Marks, R. L. Burman, M. Hamm, M. A. Moinester, R. P. Redwine, M. A. Yates, F. E. Bertrand, T. P. Cleary, E. E. Gross, N. W. Hill, C. A. Ludemann, M. Blecher, K. Gotow, D. Jenkins, and F. Milder. (1981) Positive pion-nucleus elastic scattering at 30 and 50 MeV. *Phys. Rev. C* 23:1134. DOI: 10.1103/PhysRevC.23.1134

[22] K. G. Boyer, W. J. Braithwaite, W. B. Cottingame, S. J. Greene, L. E. Smith, C. Fred Moore, C. L. Morris, H. A. Thiessen, G. S. Blanpied, G. R. Burleson, J. F. Davis, J. S. McCarthy, R. C. Minehart, and C. A. Goulding (1984) Pion elastic and inelastic scattering from ^{40,42,44,48}Ca and ^{54}Fe. *Phys. Rev. C* 29:182. DOI: https://doi.org/10.1103/PhysRevC.29.182

[23] M. Y. M. Hassan, Z. Metawei (2002) First and second order corrections to the eikonal phase shifts for the interactions of α-particle with ^{12}c and ca isotopes. *Acta Physica Slovaca*. 52: 23-34.

[24] A.A. Ebrahim and R.J. Peterson (1996) Parametrization of pion-nucleon phase shifts and effects upon pion-nucleus scattering calculations. *Phys. Rev. C* 54: 2499. DOI: https://doi.org/10.1103/PhysRevC.54.2499

[25] A. A. Ebrahim, (1997) Ph.D. Thesis, Assiut University.

[26] R. E. Chrien, R. Sawafta,, R. J. Peterson, R. A. Michael, and E. V. Hungerford (1997) Elastic and Inelastic Scattering of K+ from ^{6}Li and ^{12}C. *Nucl. Phys. A* 625:251. DOI: https://doi.org/10.1016/S0375-9474(97)00384-9

[27] D. Marlow, P. D. Barnes, N. J. Colella, S. A. Dytman, R. A. Eisenstein, R. Grace, F. Takeutchi, W. R. Wharton, S. Bart, D. Hancock, R. Hackenberg, E. Hungerford, W. Mayes, L. Pinsky, T. Williams, R. Chrein, H. Palevsky, and R. Sutter . (1982) Kaon Scattering from C and Ca at 800 MeV/c. *Phys. Rev. C* 25: 2619.

International Journal of Computational and Experimental Science and ENgineering (IJCESEN)

Vol. 8-No.2 (2022) pp. 49-55
http://dergipark.org.tr/en/pub/ijcesen

ISSN: 2149-9144

Research Article

Removal of Building Residence Area with Complex Number Approach in Free Building Identity Zoning Plots

Selim TAŞKAYA*

Artvin Coruh University, Department of Architecture and Urban Planning, 08100, Artvin-Turkey
* **Corresponding Author** : **Email:** selim_taskaya@artvin.edu.tr - **ORCID:** 0000-0002-4290-3684

Article Info:

DOI: 10.22399/ijcesen.1085694
Received : 10 March 2022
Accepted : 21 May 2022

Keywords

Free Building,
Reconstruction Island,
Zoning Status,
Complex Approach

Abstract:

The zoning blocks in the free building order are the special case of the separate, block and adjacent building regulations in the implementation zoning plans. Buildings are established in order to meet human needs in areas within the zoning boundaries by giving such building regulations. Free-order zoning parcels are another type of mostly separate and block orders. In areas where such parcels are located, only the equivalent value, which is the total construction area of the island, is usually given. Based on this precedent value, the residential area of the building is given to the parcel with various methods or approaches in accordance with the relevant law and regulation. With the complex (complex) number approach of the sample plan representations in the study, it was tried to find the tensile measures with the help of the angle, based on the direction with a certain edge. The complex approach, on the other hand, is the process of subtracting the base area on a parcel basis in a certain coordinate system axially depending on the angle and distance parameters along the Y-X axes. In this way, the necessity of giving residential areas to zoning parcels with different identities was examined.

1. Introduction

Since social life necessitates a certain order (organization) in every respect, there is a need for rules that will ensure order in every society, from the most primitive to the most advanced. As a matter of fact, various rules have been foreseen for private and public activities in society in every age. For example, in every subject such as shelter, nutrition, entertainment, work; In this sense, simple or advanced rules and regulations have been made regarding almost every human activity of economic, social and cultural nature [1]. At this point, various rules regarding settlement and construction on "soil" (supply / land and land) and regulations on zoning have been encountered for a long time [2,3]. In other words, efforts to keep settlements in order are not new [4,5]. At the point reached today, although there are different approaches to zoning and planning [6], since it does not seem possible to think of regular urbanization independently of planning, zoning planning and the basic instrument of this activity, zoning plans, with the rules brought about settlement and construction on the land, the zoning order has been determined. It can be said that it has reached the level of the main determinant [1]. Planning, as a word, is the process that regulates the order of the elements of actions directed to a certain purpose in time and their distribution in space [7]. The act of planning can be classified as economic planning, social planning, and physical planning [8]. For example, the authority to take decisions on the plans prepared in the areas within the limits of the duties, powers and responsibilities of the municipalities has been given to the municipal council, which is the general decision-making body that comes into power [7]. The fact that the municipal council has the last word in the development plans is due to the close and intense relationship of planning with fundamental rights and freedoms. It is a correct approach in terms of a democratic management approach and positive in terms of the participatory structure of planning that the development planning studies, which have the ability to create intense pressure on fundamental rights and freedoms, are decided by the city council, which was formed by the people who are the owners of these rights and freedoms [9]. In fact, zoning plans are a complex type of operation that includes both general rules

and a diagram showing the application of these rules regarding the region they cover [7]. Although the subordination of the plans to the regulatory regime with the dominant view in the jurisprudence and doctrine stems from the expression of the zoning principles and rules in a particular
region at the level of abstraction possible, it is also based on the reason that this solution has practical results [10]. Another important phase of city plans that should be emphasized at this stage is the research and analysis phase. Today, it is accepted that urban planning is no longer a static concept and is a work that has to keep up with rapid changes [11].

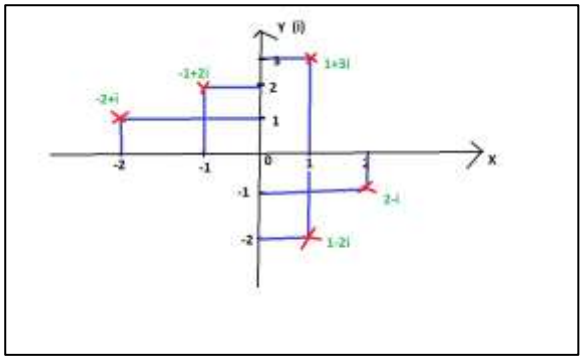

Figure 1. *Representation of Complex Plane and Complex Numbers [12].*

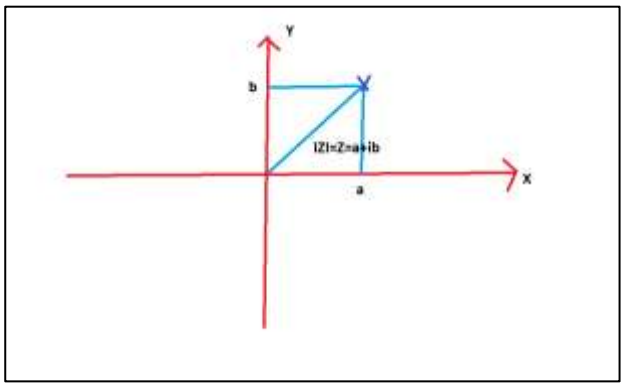

Figure 2. *Module of Complex Number [12].*

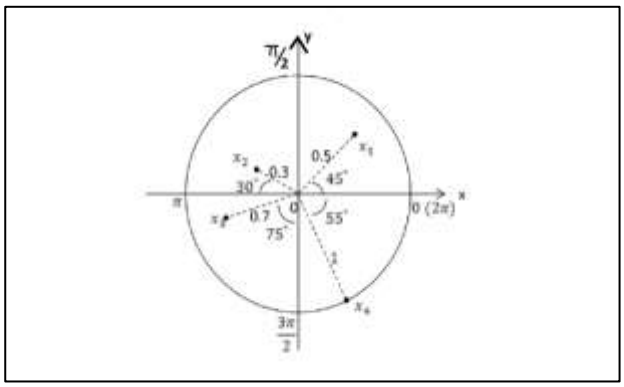

Figure 3*. Complex Fuzzy Set [12]*

2. Material and Methods

Since the plots are closed convex shapes, they have a plane area. Y and X coordinates from the junction points of both sides are found in a certain transformation system and their place is found in the geoid plane. If we show the plane mathematically here;
In Figure 1, it is seen how the convex long and short sides come together in the Y and X planes. Here, the real numbers on the Y-axis are called i when they are represented as a complex expression. The x-axis continues as real numbers
forever. From this point of view, the complex number z=a+ib can be represented as an ordered pair (a, b) [12]. The plane formed by taking the x-axis as the real axis and the y-axis as the imaginary axis is called the complex plane [12].

In Figure 2., it is seen that the distance will be calculated by pythagoras from the vertical feet and vertical lengths in the form of IZI=Z=a+ib in the Y—X plane. Given the complex number

Z=a+ib, the positive real number IZI=$\sqrt{a^2+b^2}$ is called the modulus or absolute value of the complex number zz [12].

In Figure 3., the determination of the fracture points of the parcels and the distance to the base can be calculated by means of clockwise or counterclockwise angles [12]. The aim is to determine the distance-based area and localization process from a 100 grad fixed point [13].

3. Results and Discussions

Free order parcels are the islands created by the planner as an identity open to interpretation in the zoning diameter determination processes called zoning status in the zoning plans. In these islands, especially the side and rear pull dimensions are tried to be given within the legal framework, as in the split and block types[14]. In some islands, the equivalent value may be given, and in some it may not. For those whose precedent value is not given, the process is continued by looking at the zoning islands around the relevant island. Side and rear pull measurements can be applied, such as islands with a height legend [15]. According to the regulation, the average TAKS (Base Area Coefficient) can be taken as 0.30 for those whose peer value is given, and the number of floors they correspond to can be found by making Precedent/TAKS [16].

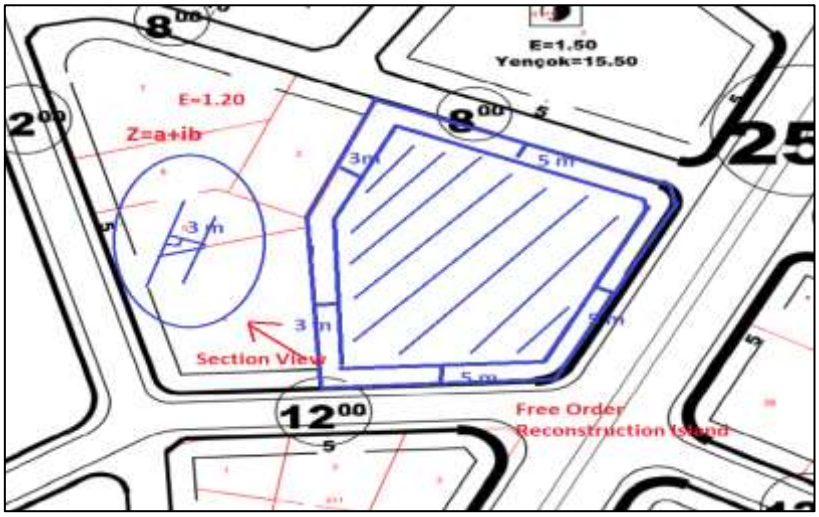

Figure 4. *A Cross-Section View of a Free Order Plot with Peer Value*

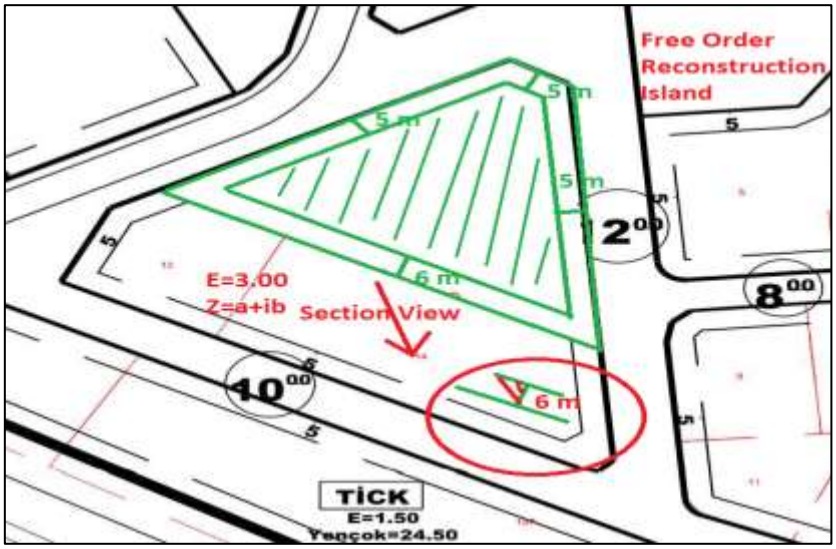

Figure 5. *Side Measurement Cross-section View of a Free Ordinary Plot*

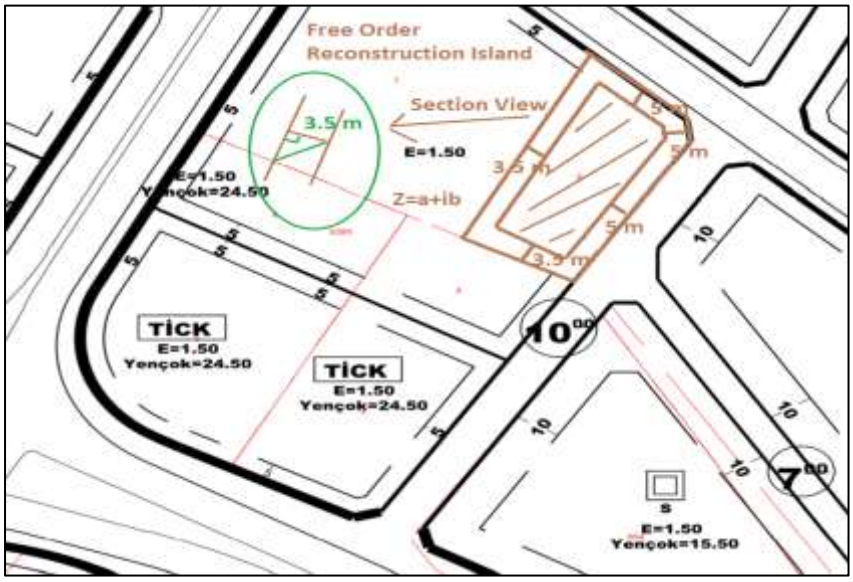

Figure 6. *Side Measurement Cross-section View of a Free Ordinary Plot*

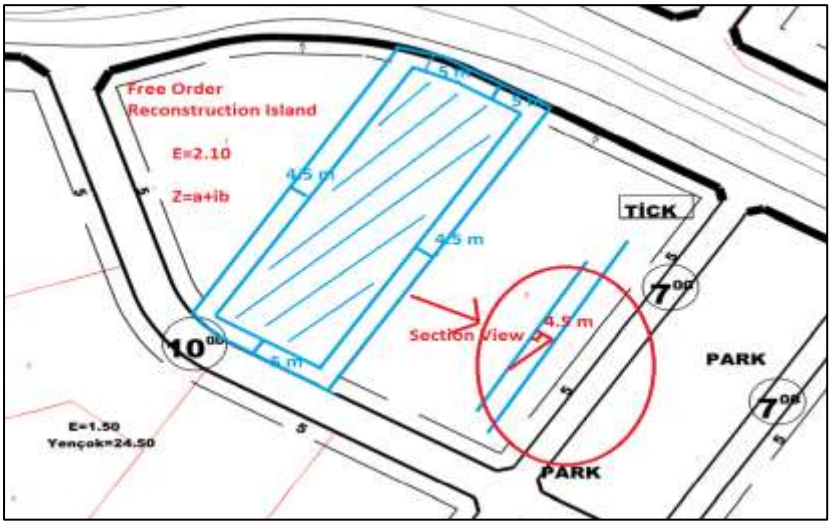

F

Figure 7. *Side Measurement 2.10 Section View of a Free Order Plot*

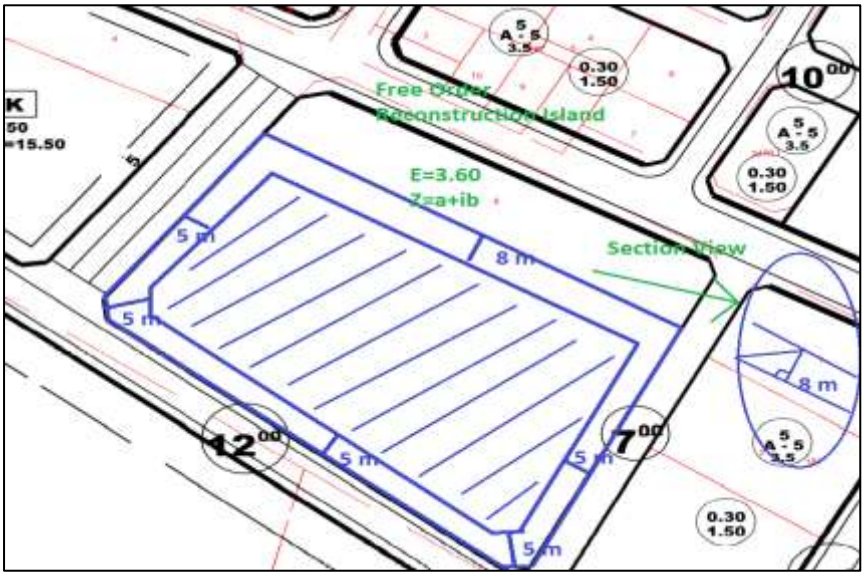

Figure 8. *Side Measurement 3.60 Section View of a Free Ordinary Plot*

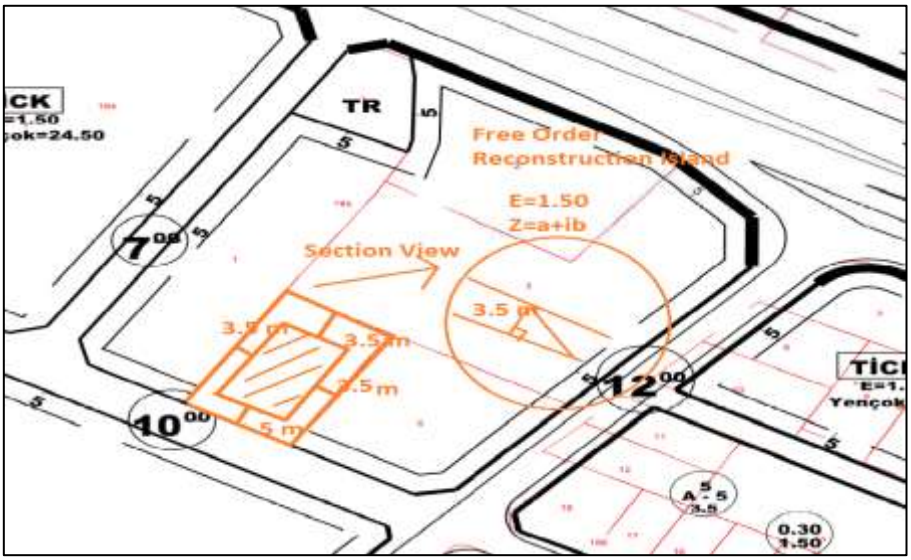

Figure 9. *Side and Back Measurement 1.50 Section View of a Free Order Plot*

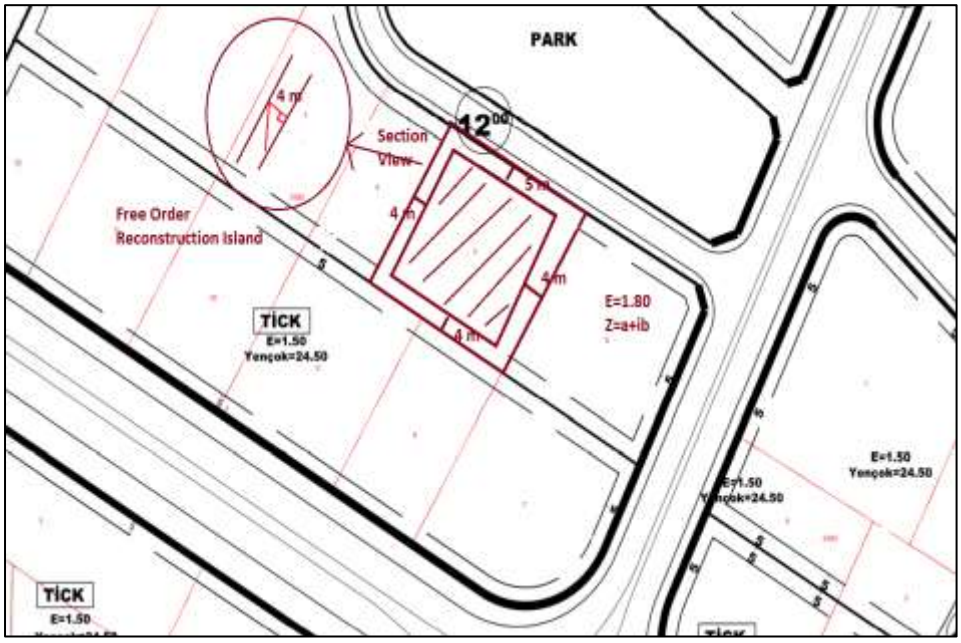

Figure 10. *Side and Back Measurement 1.80 Section View of a Free Order Plot*

If the whole surrounding is in the form of free order, the dimensions can be determined by taking a certain number of floors. The zoning parcel in Figure 4 is a large parcel in terms of area and has three sides facing the zoning roads. In this respect, it is calculated how the building will fit on the parcel in such islands. Although it is a free island, the total construction area is given. According to the planned type zoning regulation of this zoning island, which was written as 1.20 in the plan, it was noted that the average floor usage amount per floor is 0.30 [16]. From this account with an average of 0.30;

It can be found from

Equivalent Value=Total Construction Value/0.30 [17].

Since one side of this zoning parcel is bordered by the neighboring parcel, it will be drawn as 3 meters from the phrase that the side measurement will be pulled back at least 3 meters in places up to 4 floors. If there is no construction on empty plots, the front distance will be fixed 5 meters [18]. It is calculated as $Z=\sqrt{a^2+b^2}$ since the outer edge a and the inner edge ib are taken as basis in the Y-X plane from the side measurement section.

In Figure 5., the related zoning parcel will be given back to back at a single depth point, although the island is completely composed of 2 parcels, even though it is free order. As for the settlement of the building, since there is no construction on the island, a measurement of 5 meters will be made from the parts facing the road, and it will be understood that the side measurement should be made from the side, again due to the total maximum value of 3.00, which corresponds to 10 times the average equivalent. In the same way from the side section view, the edge can be determined as $Z=\sqrt{a^2+b^2}$ from the outside to the inside.

The immovable in Figure 6 is a zoning parcel located at the corner. From this point of view, since it is a point with a precedent value, 5 meters will be measured from the double-sided fixed road sections, while the side measurements will be evaluated as a point corresponding to 5 floors, and the base sitting area will be determined on the Y-X axes with 3.5 meters of drawing. The parcel in Figure 7 is the zoning parcel facing the double road in the north and south directions of the island. Since a total construction area of 2.10 will be used here, distance measurements will be made, corresponding to an average of 7 floors. The total construction area is;

*Total floor areas = Land area * Equivalent Value* [16].

Since the parts corresponding to 7 floors are side, there will be a half-meter increase per floor that is more than 4 floors, and it will be measured as 4.5 meters. It is shown from the side section view that this measurement is based on the edge from the coordinates and its availability with the help of angle. From the plan view in Figure 8., it will be deduced from our previous determinations that it corresponds to 12 floors. Since there are more than 4 floors in this parcel, which has a uniform geometric closed shape, measurement will be made from the side in the form of 8 meters, with an increase of half a meter per floor. From this point of view, the difference between $Z=\sqrt{a^2+b^2}$ can be calculated by descending 100 grads from Z=a+ib to

outer edge a to inner edge b from the 8-meter cross-section view [17]. The parcel in Figure 9. is a single-sided development parcel. Therefore, the place to stay behind is called the back area. The measurements found here, on the other hand, are evaluated as the distance to the back in line with the regulation that changed in 2017, and applications are made based on the note in the form of at least 3 meters [16]. In the image, it will be seen that the side and rear distances will be 3.5 meters when the calculation is made over 5 floors according to the 1.50 calculation in a parcel with a free building identity. It will be able to be calculated as a complex in the application process on the angle and edge bases from the outside to the inside. In Figure 10, an example is given from the parcels that are in free order, especially for the rear measurement to be certain. While determining the floor area of these parcels with a regular shape, it is seen that since the north of the island has a value of 1.80, it will correspond to 6 floors. From this point of view, the distances will be found from Z as 4 meters in the form of side and back.

4. Conclusions

In the analysis of which parameters the residential area of the building is given in the freely regulated zoning islands, these conditions have been tried to be explained with examples. According to the limits of the relevant regulation, the parcel floor was examined as a plane as a geometric approach and the distance measurements were shown. With the complex approach, plot structure base extraction is explained by considering some edges as bases and complex constants. It has been observed that in free regulations, especially on samples with known precedent values have been studied. In the absence of such sharp identification information in free orders, side and rear distance measurements should be made based on the observation of how the buildings were given in the surrounding islands, or the side and rear measurements should be determined according to a certain floor height and given below according to the following floor, the application of tension should be deducted accordingly in the increase or decrease of floors.

Author Statements:

- **Ethical approval:** The conducted research is not related to either human or animal use.
- **Conflict of interest:** The authors declare that they have no known competing financial interests or personal relationships that could have appeared to influence the work reported in this paper
- **Acknowledgement:** The authors declare that they have nobody or no-company to acknowledge.
- **Author contributions:** The authors declare that they have equal right on this paper.
- **Funding information:** The authors declare that there is no funding to be acknowledged.
- **Data availability statement:** The data that support the findings of this study are available on request from the corresponding author. The data are not publicly available due to privacy or ethical restrictions.

References

[1] Yilmaz, S., (2021). Legal Regime of Zoning Plans, Ankara University, Institute of Social Sciences, Department of Public Law, *PhD Thesis*, Ankara.

[2] Nolon, J.R., (2006). Comparative Land Use Law: Patterns of Sustainability. *Pace Environmental Law Review*, 23:862.

[3] Alterman, R., (2013). Planning Laws, Development Controls, and Social Equity: Lessons for Developing Countries. *The World Bank Legal Review*, 5:344.

[4] Yayla, Y.,(1975). Major Legal Issues of Urban Planning and the Case of Istanbul, *IU Pub*., Istanbul, p.10.

[5] Jacquignon, L., (1967). Naked from Le Droit de l'Urbanisme, *Paris*, p.6-7.

[6] Arikan, Y.E., (1999). Searching for a New Framework for the Restructuring of the Planning Institution. *Metropolitan Areas Planning Problems I. Symposium Proceedings*, 15-16 October 1998, Yıldız Technical University Pub., Istanbul, p.311.

[7] Topal, H.K., (2019). Limitation of Property Rights Through Development Plans, *Yaşar University, Institute of Social Sciences, Department of Private Law*, Master's Thesis, İzmir.

[8] Arkon, C., (2006). City Planning/Design Dictionary, *Meta Press*, İzmir.

[9] Colak, N., (2014). Zoning Law, Istanbul, Revised and Enlarged 2nd Edition, p.277.

[10] Tekinsoy, M. A., (2008). Legal Quality of Zoning Plans, Effect of Cancellation of Zoning Plan on Licenses Granted Based on this Plan, *Journal of Ankara Bar Association*, 66(2):46-56.

[11] Çiçek, K., (2016). Principles and Procedures of Zoning Plan Changes, Istanbul Commerce University, *Institute of Social Sciences, Department of Public Law*, Master's Thesis, Istanbul.

[12] Yigit, N., (2018). Complex Fuzzy Sets and Applications, Tokat Gaziosmanpaşa *University, Department of Mathematics*, Master Thesis, Tokat.

[13] Anonymous Publications, (2021). Lecture Notes on the Subject of Mathematics Complex Numbers.

[14] Taşkaya, S., (2021a). Zoning Diameter Display According to Distance Approach in Residential Commercial Development Islands, *Gaziosmanpaşa Journal of Scientific Research*, 10(3):217-228.

[15] Taşkaya, S., (2021b). Determination of Zoning Diameter by Distance Method in Reconstruction Islands whose Height Coefficients are Only Legend, *Journal of Design, Architecture and Engineering*, 2(1):36-45.

[16] Planned Type Zoning Regulation, (2017). Official Gazette Date: 03.07.2017, Number: 30113.

[17] Taşkaya, S., (2021c). Representation of Zoning Diameter by Distance Approach in Commercial Zoning Islands, *Journal of Istanbul Sabahattin Zaim University Institute of Science and Technology*, 3(3):204-211.

[18] Taşkaya, S., (2021d). Zoning Diameter Representation According to Distance Approach in Fuel Reconstruction Islands, *Recep Tayyip Erdoğan University Journal of Science and Engineering* 2(2):51-59.

International Journal of Computational and Experimental Science and ENgineering (IJCESEN)
Vol. 8-No.2 (2022) pp. 56-58
http://dergipark.org.tr/en/pub/ijcesen

ISSN: 2149-9144

Research Article

A Teaching Method for the Natural Sciences

Naim SYLA[1], Jürgen SCHONHERR[2†] Edina MALKIC[3] and Fisnik ALIAJ[4*]

[1]University of Prishtina, Department of Physics, Pristina –KOSOVO
Email : naim.syla@uni-pr.edu **ORCID:** 0000-0003-0857-4685

[2]GERMANY (died from COVID19 in December 2020)
Email : nsyla1964@gmail.com **ORCID:** 0000-0003-0857-4685

[3]MU "Interaktivne otvorene skole" Ul. Pozorišna 13,75 000 Tuzla, B&H,
Email: muios@bih.net.ba **ORCID:** 0000-0003-0857-4685

[4] University of Prishtina, Department of Physics, Pristina –KOSOVO
* **Corresponding Author Email** : fisnik.aliaj@uni-pr.edu **ORCID:** 0000-0002-9967-8334

Article Info:

DOI: 10.22399/ijcesen.1034925
Received: 17 December 2021
Accepted: 09 June 2022

Keywords
Experiment,
Starter Approach,
Natural Sciences,
Mathematics

Abstract:

In this contribution, we will introduce a new method of teaching and learning for the natural sciences (Biology, Physics, Chemistry) and Mathematics. The inventor and practical implementer in several world countries (Indonesia, Tanzania, Kosovo, Kyrgyzstan, Kazakhstan, Bosnia & Herzegovina, and some schools in Germany) was Jürgen Schőnherr. The philosophy of this method is based on the idea that the first lesson of each chapter begins with an experiment, which should be clear, simple (built with ordinary tools from students' lives, kitchens, toys, tools, etc.), and have a surprising effect. Based on this approach, the method is also called Starter Experiment Approach. The role of the teacher during this lesson will be more of a guide and helper, while most of the time will belong to the students. Thus, students will be aroused with curiosity and love for natural sciences. In countries where this method has been applied, positive effects have been observed in increasing the number of researchers in the natural sciences, and their success.

1. Introduction

Most research in natural sciences and technology depends on the design and implementation of the research experiment [1-5]. Given the importance of experimentation in the natural sciences and technology, different teaching methods and mathematics methods have recently been developed. These methods are applied from primary school, when students firstly have contact with subjects such as physics, chemistry, biology and mathematics [6-11]. One of the most important methods, which has shown practical results [7,8], is undoubtedly the one we will present in the following.

The name "Starter Experiment" was chosen to indicate two things [7]:
The process of teaching/learning in science has to **start** from the observation of phenomena, either obtained from the environment or an experiment (Martin Wagenschein).

Starting a new chapter of the syllabus or in the textbook shall be based on students' observations of natural phenomena, or derived from a "Starter-Experiment". For their explanations, they are using their pre-concepts / pre-knowledge, which will be confronted with the science concepts in the course of the 'SEA-lesson'. These concepts will be developed by students as a result of their investigations to test their hypotheses for correctness. Thus, new concepts are developed as a result of the teaching/learning process, correspondingly, the new concepts are replacing incorrect pre-concepts (Jean Piaget: Restructuring). This way, students will avoid developing two unconnected sets of knowledge; one they use for getting along in their environment, in their daily life, in the family and community, and the other one to cope with the demands in school. For this purpose, each chapter of the syllabus should be started, if possible, by this approach.

"Re-uniting" students' worlds -their environment and the school- makes learning meaningful and motivating for them. Both being the precondition of the improvement of the teaching / learning process esp. in science subjects.

2. The Steps of the Approach

The Starter Experiment Approach follows the "Scientific Cycle" * [7,8]:

1. Observing phenomena either directly in the environment or through an experiment;
2. Attempting to Explain why certain things were observed, students using their pre-concepts;
3. Verifying/Falsifying the attempted explanations (hypotheses) by means of experiments, preferably designed by the students themselves;
4. Assessing the attempted explanations by means of the results of the verification experiments;
5. a) Formulating a Concept in case of a positive assessment of the hypothesis. Or b) Formulating a New Hypothesis in case of a negative assessment of the original hypothesis followed by a new verification process;
6. Linking the Concept to students' environment and its applications in technology and science;
7. Evaluating students' degree of comprehension of the newly found concept.

***) T**here is a slightly different procedure for mathematics.

3. Teaching with the Starter Experiment Approach

To teach science while using this approach successfully, the teacher needs to undergo a training covering both, methodology and contents. Since this approach is very different from what teachers are used to doing, the training must also provide them with a considerable self-confidence in their ability to apply the new strategy. After having undergone the training -the training itself is described under the chapter "Training Structure"- the teachers are expected to conduct science lessons following this very approach at least each time when they ***start*** with a new chapter of the syllabus. Thus, students will develop a high degree of motivation, which will last for the periods to follow, even if the teacher falls back to more traditional ways of instruction. However, it is important that frequent references are made to the initial Starter Experiment for this chapter. This way the motivation can be sustained for a long time.

4. Effects of SEA on Students and Teachers

Teachers applying this method will experience a change in students' attitude towards science subjects and mathematics: Students will start investigating questions outside the actual science lesson, e.g., by designing and conducting their own experiments at home. Students will bring "improvised equipment" to the school to demonstrate certain experiments they have "invented". Students will utter their satisfaction with the subject, and will include their science and/or mathematics teacher in such statements. In turn, teachers will observe some changes in their own attitude towards the lessons they have to give. They will observe that they spend more time thinking about these lessons, they will spend more time preparing them, they will become more open to students' questions and suggestions, and they will find teaching satisfactory and rewarding...

Some other effects frequently observed [7,8]:

- Students become more tolerant towards deviating ideas of classmates.
- Students become more supportive among each other.
- Girls are more respected and are actively involved in lessons traditionally regarded as the domains of boys.
- The positive attitude towards science subjects and mathematics ***spills over*** to other subjects.
- Due to the training element ***Mutual Monitoring*** the cooperation of teachers increases.

5. The Training Structure

At the first step of the training, participants are exposed to a lesson following the steps of the Starter-Experiment-Approach. They experience the desired teaching/learning process in the role of students, the trainer being the "model-teacher".
This is followed by analyzing the approach step by step, and backing them up by short lectures about learning psychology, the way knowledge is created. Here participants find themselves in the role of college students. Based on the experience gained in the previous steps, participants are asked to select a topic from the curriculum and to prepare a lesson following the new approach, still in the role of college students.
In the role of teacher, each participant is given the chance to tryout the lesson they have planned in a "Peer-Teaching" session, whereby the other participants are acting as students. During the peer-teaching performances the trainer acts as a

monitor, modelling the way effective monitoring can be done. In the course of the peer-teaching exercises, the trainer involves the participants successively in monitoring the demonstrating colleague. They now take part in two roles: The role of student and the role of monitor. To reduce the fear to fail when applying the new approach back in their schools all participants will teach "their lesson" in a normal class with normal students. One participant is the teacher, the remaining participants act as monitors. Thus, self-confidence increases, the fear to fail vanishes. Back in their schools' participants have to apply the new approach for at least six times within the following 6 to 9 months. These "SEA-lessons" must be monitored by one colleague who has also undergone the SEA-training. After 6 to 9 months' participants attend a refresher seminar. Here participants discuss their experience gained by applying SEA in their schools, focusing on problems/difficulties observed, and developing adaptations to overcome them, meanwhile, the trainer acting mainly as organizer and source of ideas.

6. Conclusions

- The SEA method is suitable and effective for the natural and mathematical sciences.
- Starts to apply from primary school and especially from the fifth grade
- It is easily feasible because it does not require special laboratory equipment (tools are taken from the daily life of students).
- The results prove that, by applying this method, the students' interest in natural sciences increases, and what is more important, the prejudices that natural and mathematical sciences are difficult fall [7].

Author Statements:

- **Ethical approval:** The conducted research is not related to either human or animal use.
- **Conflict of interest:** The authors declare that they have no known competing financial interests or personal relationships that could have appeared to influence the work reported in this paper
- **Acknowledgement:** Authors want to thank Jürgen Schönherr - Papa SEA (already deceased), Am Grundweg 82, D-64342 Seeheim-Jugenheim, Germany, who was the inventor of this method. From all the materials that Jürgen had prepared for the various trainings, the authors are summarized in this article.
- **Author contributions:** The authors declare that they have equal right on this paper.
- **Funding information:** The authors declare that there is no funding to be acknowledged.
- **Data availability statement:** The data that support the findings of this study are available on request from the corresponding author. The data are not publicly available due to privacy or ethical restrictions.

References

[1] A. Kaouka et al. (2020), Characterization and Properties of Boriding Titanium Alloy Ti6Al4V. *Acta Physica Polonica A*137(4):493-495 DOI: 10.12693/APhysPolA.137.493

[2] I. Bozetine eta al. (2020), Study of the Influence of the Annealing Temperature on the Properties of SiC-SiO2 Thin Films, *Acta Physica Polonica* A137(4):499-501 DOI: 10.12693/APhysPolA.137.499

[3] İ.H. Kara eta al. (2020), Effect of Ca and Ce on Wear Behavior of Hot-Rolled AZ31 Mg Alloys, *Acta Physica Polonica* A137(4):557-560 DOI: 10.12693/APhysPolA.137.557

[4] H. Ahmad Mukifza eta al. (2017), Experimental Analysis of Titanium Dioxide Synthesis from Synthetic Rutile Waste using a Moderate Acid Concentration and Temperature, *Acta Physica Polonica* A132(3II):833-835 DOI: 10.12693/APhysPolA.132.833

[5] N. Syla et al, (2017) Hardness Curves for 31CrMoV9 Steel after Gas Nitriding. *Acta Physica Polonica* A132(3):484-486 DOI: 10.12693/APhysPolA.132.484

[6] Brekke, M., Hogstad, P.H. (2010), New teaching methods - using computer technology in physics, mathematics and computer science. *Int. J. Digital Soc.*, 1

[7] Naim Syla, Gezim Hodolli (2017), The teachıng method named "Starter-experıment-approach", Chemistry: *Bulgarian Journal of Science Education*, 26:6.

[8] Indrayati, N.K., Renda, N.T. & Sudarma, I.K. (2014). Pengaruh model pembelajaran starter eksperiment approach terhadap keterampilan proses sains. *e-J. MIMBAR PGSD Universitas Pendidikan Ganesha Jurusan PGSD,* 2(1).

[9] Kitta, S. (2015). Development of mathematics teachers: experience from Tanzania. *Int. J. Educ. Sci.*,

[10] Mistler-Jackson, M. & Songer, N.B. (2000). Student motivation and internet technology: are students empowered to learn science. *J. Res. Sci. Teaching,* 37:459 – 479.

[11] Niess, M.L. (2005). Preparing teachers to teach science and mathematics with technology: developing a technology pedagogical content knowledge. *Teaching & Teacher Edu*c., 21:509 – 523.